Defence Technology 17 (2021) 100–118

Contents lists available at ScienceDirect

Defence Technology

journal homepage: www.keaipublishing.com/en/journals/defence-technology

A higher order coupled frequency characteristics study of smart magneto-electro-elastic composite plates with cut-outs using finite element methods

M. Vinyas [a, *], D. Harursampath [a], T. Nguyen Thoi [b, c]

[a] Nonlinear Multifunctional Composites Analysis and Design (NMCAD) Laboratory, Department of Aerospace Engineering, Indian Institute of Science, Bangalore, 560012, India
[b] Division of Computational Mathematics and Engineering, Institute for Computational Science, Ton Duc Thang University, Ho Chi Minh City, Viet Nam
[c] Faculty of Civil Engineering, Ton Duc Thang University, Ho Chi Minh City, Viet Nam

ARTICLE INFO

Article history:
Received 3 December 2019
Received in revised form
17 January 2020
Accepted 12 February 2020
Available online 20 February 2020

Keywords:
Cut-out
Magneto-electro-elastic
Natural frequency
Higher order shear deformation
Coupling

ABSTRACT

This article deals with investigating the effect of cut-outs on the natural frequencies of magneto-electro-elastic (MEE) plates incorporating finite element methods based on higher order shear deformation theory (HSDT). In order to consider the influence of cut-out, the energy of the cut-out domain is subtracted from the total energy of the entire plate. The governing equations of motions are derived through incorporating Hamilton's principle and the solution is obtained using condensation technique. The proposed numerical formulation is verified with the results of previously published literature as well as the numerical software. In addition, this research focuses on evaluating the effect of geometrical skewness and boundary conditions on the frequency response. The influence of cut-outs on the degree of coupling between magnetic, electric and elastic fields is also investigated.

1. Introduction

Magneto-Electro-Elastic (MEE) materials belong to the class of unique smart materials which exhibit superior magneto-electric coupling and triple energy conversion capabilities which are usually not witnessed in individual piezoelectric or piezomagnetic materials [1,2]. Further, the MEE structures tend to improve the multifunctionality when subjected to different working environments [3–8]. Due to this nature of MEE materials numerous engineering applications are benefited. Many researchers have attempted to investigate the mechanical responses of the smart MEE structures. Among them, Pan and his fellow researchers [9,10] demonstrated the vibration characteristics of anisotropic MEE plate via exact solutions. Wang et al. [11] and Chen et al. [12] probed the natural frequencies of MEE plate through state vector approach. Lage et al. [13] adopted mixed layer-wise finite element (FE) method to solve the problem of dynamic analysis of MEE plates. Alongside, other methods which have claimed to be efficient in solving the free vibration problem of MEE plates include approximate solution method [14,15], semi-analytical FE procedure [16], FE methods [17,18], meshless method [19] and state space approach [20–22]. The effectiveness of MEE structures in vibration damping is also reported in the literature [23–26]. Vinyas et al. [27] proposed a FE formulation in the frame work of first order shear deformation theory (FSDT) to evaluate the influence of different coupling fields on the free vibration characteristics of magneto-electro-thermo-elastic (METE) plates. However, the FSDT additionally requires shear-correction factor (SCF) in order to correct the transverse shear stress and to obtain the correct energy. In this regard, higher order shear deformation theory (HSDT) proves handy and the structural kinematics can be expressed in a better way. A minimal work has been reported on assessing the free vibration response of MEE plates using HSDT. Moita et al. [28] researched the natural frequency of MEE plate using HSDT. Shooshtari and Razavi [29] exploited HSDT to determine the effect of elastic foundation on the vibrations of MEE plate. Vinyas and co researchers developed a FE

* Corresponding author. Department of Aerospace Engineering, Indian Institute of Science, Bangalore, 560012, India.
E-mail addresses: vinyasmahesh@iisc.ac.in, Vinyas.mahesh@gmail.com (M. Vinyas).
Peer review under responsibility of China Ordnance Society

https://doi.org/10.1016/j.dt.2020.02.009

formulation incorporating HSDT to investigate the influence of hygrothermal loads [30,31], geometrical skewness [32], Carbon Nano-tube reinforcements [33] and piezoelectric interphase [34] on the natural frequency of MEE plates. More recently, the coupled frequency response of annular MEE plates using FE methods was proposed by Vinyas et al. [35] under the framework of HSDT.

In the various engineering applications, the perforated plates or plates with cut-outs are most commonly used. Vibration analysis of plates with discontinuities or cutouts shows commendable variation with respect to that of normal plates. The differences are primarily attributed to the geometric dimensions of the cutout, its location, and other factors. By introducing cut-out in the structures, the weight and hence the dynamic characteristics of the entire structure significantly alters. Therefore it is very crucial to assess the frequencies of the structures with cut-outs. Various studies conducted in the past have provided a number of computational methods which have been proven to be efficient. Through Rayleigh-Ritz method, the natural frequencies of rectangular plates with circular [36] and rectangular holes [37,38] were evaluated. Similar objectives were accomplished with the aid of finite element methods effectively [39–41]. The influence of in-plane loads and cut-outs on the vibration characteristics of square plates and rectangular plates was evaluated by Lee et al. [42] and Huang [43], respectively. Lee et al. [44] extended their study to assess the effects of transverse shear deformation and rotary inertia also. The study concluded that the effect of rotary inertia became more pronounced with increasing cutout sizes. Nguyen et al. [45] analyzed the natural frequency response of functionally graded plates with complex cutouts using the isogeometric approach (IGA) and quasi-3D HSDT. Wang et al. [46] proposed a unified approach to study the free vibrations of elastically restrained plates with holes. Through singular perturbation technique, Andrianov et al. [47] addressed the dynamic problem of elastic plates and membranes with periodically perforated holed. Chen et al. [48] utilized boundary element method (BEM) for vibration analysis of 2-D anisotropic elastic solids containing holes. Chebyshev-Lagrangian method was exploited by Chen et al. [49] to assess in-plane vibrations of plate with cutout under general boundary conditions. Hota and Padhi [50] used sub parametric triangular plate bending element in association with FSDT to evaluate the effect of irregular cutouts on the vibration response. Also, independent coordinate coupling method has been found useful in studying the free vibration of a specially orthotropic composite laminate with rectangular or circular cutout at the laminate centre [51]. Liew et al. [52] proposed the discrete Ritz formulation to obtain the vibration frequencies and mode shapes of the plates. Sandwiched composite plates with holes at various locations are affected by the core and face sheet thicknesses, diameter and location of holes and the aspect ratio of the plate as shown by Mondal et al.[53]. Shufrin et al.[54] demonstrated the usage of the extended Kantorovich method for free vibration analysis of rectangular plates with a combination of variable thickness and cutouts. Similarly, HSDT and Hamilton's principle based FE approach was used to analyze the free vibrations of square laminates with a central rectangular cutout [55]. A comparison of the results with FSDT revealed that the natural frequencies are higher in the case of the HSDT. This difference increases with the increasing mode number. By employing HSDT, Lee [56] studied the dynamic stability of laminated composite skew plates with cutouts sand subjected to in-plane pulsating loads. Similarly, Park et al.[57] studied the free vibrations of laminated composite skew plates having delamination around a central quadrilateral cutout. The influence of hazardous environment on the structural response of composite laminates with cut-outs is also reported in the literature [58,59]. Based on finite strip method, the frequency response of composite plates with cutout was studied by Ovesy and Fazilati [60]. Zhang et al. [61] developed the Hencky bar – net model (HBM) to be a physical structural representation of the finite difference model (FDM) for vibration analysis of rectangular plates with cutouts of the same geometry. Also, a finite-strain geometrically exact plates and shell models [62,63] can be exploited for the analysis of smart laminated structures, due to its higher computational accuracy.

Particularly in case of MEE structures, the plates with cut-out may be highly useful to resolve space constraints in sensor and actuator application where there is a necessity to accommodate other components in a minimum space. Analogous to composite or isotropic plates the dynamics properties of MEE plates also varies with cut-outs. Alongside, the coupling capabilities are significantly altered. However, to the best of authors' knowledge the influence of coupled field interaction on the vibrations of MEE plates with cut-out is not well-investigated. In this regard, a FE formulation based on HSDT is proposed for the first time in the open literature. Meanwhile, the results of this study are also compared with that of the COMSOL solutions. Also, a special attention is paid on investigating the effect of geometrical skewness and different cut-out dimension on the coupling frequency.

1.1. Problem description

This work considers three layered MEE rectangular and skew plates with different cut-out dimensions for evaluation. Based on the arrangement of the piezoelectric (B) and piezomagnetic (F) phases, the stacking sequences are bifurcated into B/F/B and F/B/F arrangement. The schematic representation of the layered MEE plate with cut-out is shown in Fig. (1). Let us assume a MEE plate with length a in x-direction, width b in y-direction and thickness h. Also, a_c, b_c represents the length and width of the cut-out, respectively. In addition, λ denotes the skew angle of the plate. The material properties of piezoelectric and piezomagnetic phases are tabulated in Table 1.

1.2. Plate kinematics and finite element formulation

The higher order shear deformation theory (HSDT) is employed to establish the displacement field of MEE plate with cut-out problem [30]:

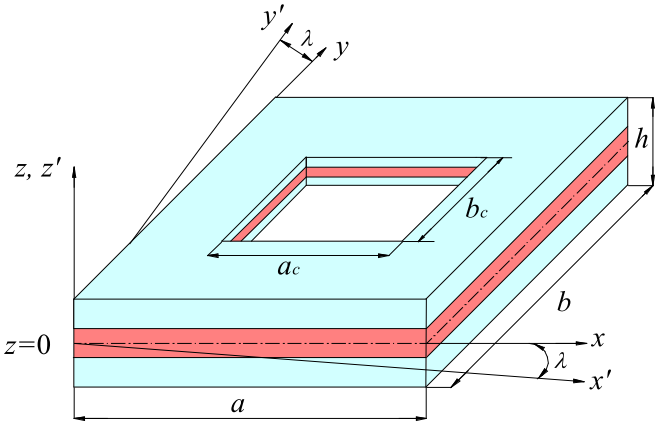

Fig. 1. Schematic of MEE plate with cut-out.

Table 1
Material properties of $BaTiO_3$–$CoFe_2O_4$ composite w.r.t different volume fraction V_f of $BaTiO_3$–$CoFe_2O_4$Vinyas and Kattimani [32].

Material property	Material constants	Piezomagnetic (F)	Piezoelectric (B)
Elastic constants (GPa)	$C_{11} = C_{22}$	286	166
	C_{12}	173	77
	$C_{13} = C_{23}$	170	78
	C_{33}	269.5	162
	$C_{44} = C_{55}$	45.3	43
	C_{66}	56.5	44.5
Piezoelectric constants (C/m^2)	e_{31}	0	−4.4
	e_{33}	0	18.6
	e_{15}	0	11.6
Dielectric constant (10^{-9} C^2/Nm^2)	$\varepsilon_{11} = \varepsilon_{22}$	0.08	11.2
	ε_{33}	0.093	12.6
Magnetic permeability (10^{-4} Ns^2/C^2)	$\mu_{11} = \mu_{22}$	−5.9	0.05
	μ_{33}	1.57	0.1
Piezomagnetic constants (N/Am)	q_{31}	580	0
	q_{33}	700	0
	q_{15}	560	0
Magneto-electric constant (10^{-12}Ns/VC)	$m_{11} = m_{22}$	0	0
	m_{33}	0	0
Density (kg/m^3)	ρ	5300	5800

$$u = u_0 + z\theta_x - \frac{4}{3h^2}z^3\left(\theta_x + \frac{\partial w_0}{\partial x}\right)$$
$$v = v_0 + z\theta_y - \frac{4}{3h^2}z^3\left(\theta_y + \frac{\partial w_0}{\partial y}\right) \quad (1)$$
$$w = w_0$$

where, $z = 0$ is considered as the reference plane. Also, the displacement components along x, y, and z-axes of this reference plane is represented by u_0, v_0, and w_0, respectively. The transverse normal rotations to the xz plane and yz plane are denoted by θ_x and θ_y, respectively.

The geometry of the plate is discretized using eight-noded isoparametric element. The displacement degrees of freedom are differentiated into translational, rotational and higher-order displacements and expressed through shape functions as follows:

$$\{d_{ti}\} = [u_i\ v_i\ w_i]^T,\ \{d_{ri}\} = [\theta_{xi}\ \theta_{yi}]^T,\ \{d_{r*i}\} = [\kappa_{xi}\ \kappa_{yi}]^T$$
$$\{d_t\} = [N_t]\{d_t^e\},\ \{d_r\} = [N_r]\{d_r^e\},\ \{d_r\} = [N_r]\{d_r^e\} \quad (2)$$
$$\varphi = [N_\varphi]\ \{\varphi^e\},\ \psi = [N_\psi]\ \{\psi^e\}$$

In addition, the remaining degrees of freedom like electric potential and magnetic potential can be represented as

$$\varphi = [N_\varphi]\ \{\varphi^e\},\ \psi = [N_\psi]\ \{\psi^e\}$$

The linear strains can be differentiated as bending $\{\varepsilon_b\}$ and shear strain $\{\varepsilon_s\}$ and its relationship with the displacement parameters ($\{d_t^e\}$, $\{d_r^e\}$ and $\{d_{r*}^e\}$), can be expressed under the framework of HSDT as [21]:

$$\{\varepsilon_b\} = [B_{tb}]\{d_t^e\} + z[B_{rb}]\{d_r^e\} + c_1 z^3[B_{rb}]\{d_r^e\} + c_1 z^3[B_{rb}]\{d_{r*}^e\}$$
$$\{\varepsilon_s\} = [B_{ts}]\{d_t^e\} + [B_{rs}]\{d_r^e\} + c_2 z^2[B_{rs}]\{d_r^e\} + c_2 z^2[B_{rs}]\{d_{r*}^e\} \quad (3)$$

Also, the relationships are established between electric intensity and electric potential; magnetic field and magnetic potential incorporating Maxwell's electro-static equations as follows:

$$\{E\} = [B_\varphi]\{\varphi^e\};\ \{H\} = [B_\psi]\{\psi^e\} \quad (4)$$

The various matrices appearing in Eqs. (2)–(4) are explicitly represented in Appendix. The readers are encouraged to go through the authors own work [35] for more details on FE procedure adopted.

1.3. Hamilton's principle

The overall energy E_{pc} of the MEE plate with cut-out can be obtained by subtracting the energy E_c of the cut-out from the E_P of the MEE plate without cut-out. To this end, the Hamilton's principle can be represented as follows [51]:

$$E_{pc} = E_p - E_c \quad (5)$$

where,

$$E_p = \frac{1}{2}\sum_{n=1}^{N}\int_{\Omega_p^n}\delta\{\varepsilon_b\}^T\{\sigma_b\}d\Omega_p^n + \frac{1}{2}\sum_{n=1}^{N}\int_{\Omega_p^n}\delta\{\varepsilon_s\}^T\{\sigma_s\}d\Omega_p^n -$$
$$\frac{1}{2}\sum_{n=1}^{N}\int_{\Omega_p^n}\delta\{E\}^T\{D\}d\Omega_p^n - \frac{1}{2}\sum_{n=1}^{N}\int_{\Omega_p^n}\delta\{H\}^T\{B\}d\Omega_p^n + \int_{\Omega_p^n}\delta\{d_t\}\rho\{\ddot{d}_t\}d\Omega_p^n \quad (6)$$

$$E_h = \frac{1}{2}\sum_{n=1}^{N}\int_{\Omega_h^n}\delta\{\varepsilon_b\}^T\{\sigma_b\}d\Omega_h^n + \frac{1}{2}\sum_{n=1}^{N}\int_{\Omega_h^n}\delta\{\varepsilon_s\}^T\{\sigma_s\}d\Omega_h^n -$$
$$\frac{1}{2}\sum_{n=1}^{N}\int_{\Omega_h^n}\delta\{E\}^T\{D\}d\Omega_h^n - \frac{1}{2}\sum_{n=1}^{N}\int_{\Omega_h^n}\delta\{H\}^T\{B\}d\Omega_h^n + \int_{\Omega_h^n}\delta\{d_t\}\rho\{\ddot{d}_t\}d\Omega_h^n \quad (7)$$

in which, Ω_p^n and Ω_h^n denotes the total volume of the plate without cut-out and the hole, respectively. Further, n and N represents layer number and total number of layers. Substituting Eqs. (1)–(4) and Eqs. (6) and (7) in Eq. (5) and adopting condensation technique, the global coupled equations of the MEE plate with cut-out can be expressed as

$$[M_{eq}]\{\ddot{d}_t\} + [K_{eq}]\{d_t\} = 0 \quad (8)$$

The detailed derivation of Eq. (8) is explicitly described in Appendix.

2. Results and discussion

In this section the natural frequency analysis of MEE plate with cut-out has been carried out through the FE formulation derived previously. As a first step, the convergence and comparative study is performed with the aid of the proposed FE formulation and COMSOL software. As depicted in Table 2, the results of the fundamental natural frequency converge very well for the proposed FE formulation, with minimum computational time and reduced degrees of freedom as opposed to the commercial software. This upholds the benefit of the proposed formulation. In addition, the results from the present formulation are compared with COMSOL software and presented in Table 3. It can be witnessed that the results matches very well which justifies the credibility of the proposed FE formulation to incorporate coupled fields accurately. Due to lack of literatures reported on evaluating the coupled frequency of MEE plate with cut-out, the verification of the FE formulation is carried out with the free vibration problem of composite plate with cut-out as illustrated in Venkateshappa et al. [64]. To this end the proposed FE formulation in uncoupled state (only elastic fields are considered) is used. Also, the similar material and geometrical properties considered in Ref. [64] is adopted for the verification. From Table 4 it is clearly evident that the proposed formulation exhibits a close correlation with the previously published experimental as well as numerical results. Hence, from these two verifications the credibility of the proposed formulation to incorporate the coupling fields as well as the cut-outs is justified.

Table 2
Convergence of the fundamental natural frequency of MEE plate with mesh size (BFB, $\lambda = 0^{\circ}$; $a_c = b_c = 0.3$ m; CCCC).

Mesh Size	Computation Time (s)	No. DOF	No. Elements	Frequency (Hz)
Present FE method				
5 × 5	10.18	720	16	1630.5
10 × 10	24.16	2304	64	1634.2
15 × 15	68.61	4752	144	1637.3
20 × 20	96.45	9180	300	1639.2
25 × 25	147.5	15138	504	1639.3
COMSOL solutions				
Coarser	65.87	6459	841	1622.3
Coarse	89.72	12324	1023	1637.4
Normal	154.1	42234	4234	1639.8
Fine	257.2	67833	10223	1641.3
Finer	463.2	154654	22332	1641.5

Table 3
Verification of the natural frequencies of MEE plate with cut-out ($\lambda = 0^{\circ}$; $a_c = b_c = 0.3$ m; CCCC).

Mode Number	BFB		FBF	
	Present	COMSOL	Present	COMSOL
1	1639.3	1641.5	1780.8	1781.3
2	2041.7	2043.2	2396.8	2398.6
3	2112.4	2113.8	2403.5	2405.5

Table 4
Verification of the proposed FE formulation with the non-dimensional frequency coefficient of antisymmetric composite plates.

Mode Number	aca = 0.1			aca = 0.3		
	FEM [64]	Exp [64].	Present	FEM [64]	Exp [64].	Present
1	6.9467	6.7383	6.8531	7.2067	6.9905	7.1092
2	7.4771	7.2528	7.3134	7.4713	7.2471	7.3418
3	11.1477	10.8133	11.084	11.2603	10.9225	11.253

2.1. Effect of cut-out dimension

The influence of cut-out on the natural frequencies of MEE plate with all sides clamped (CCCC) is analyzed. To this end, the following plate dimensions are selected: $a = b = 1$ m; $h = 0.3$ m. The variation of the first three natural frequencies with different cut-out dimensions ($a_c = b_c$) and stacking sequence is depicted in Table 5. From these results it is distinctly clear that in contrast to the MEE plate without cut-out, the natural frequencies improve as the cut-out dimension increases. The probable reason may be that as opposed to the plate without cutout, the simultaneous reduction of mass and stiffness occur for the MEE plate with cut-out. However, the dominant effect of mass reduction over the stiffness reduction is noticed. Therefore, the natural frequencies tend to increase. Meanwhile, in contrast to BFB stacking sequence, a significant effect of FBF stacking sequence in association with the cut-out dimensions on the frequencies is noticed. The first six mode shapes of the rectangular MEE plate corresponding to various cut-out dimensions are shown in Fig. 2(a).

2.2. Effect of skew angle and boundary condition

The geometrical skewness significantly affects the natural frequency of the MEE plate due to reduced area and improved stiffness. However, its effect associated with different cut-out dimension on the coupled natural frequency is very crucial to investigate. To this end, MEE plate with CCCC condition is considered for evaluation. The results illustrated in Table 6 clearly signify that with the increase in skew angle and cut-out dimension of the MEE plate the natural frequencies drastically increases. The mode shapes corresponding to different skew angles and cut-out dimensions of MEE plate with CCCC condition is explicitly illustrated in Fig. 2(b)–(d).

The investigation is extended to study the effect of boundary conditions associated with skew angles and cut-out dimensions. To this end, along with CCCC boundary condition, the influence of adjacent sides (one straight edge and one skewed edge) clamped (CCFF) and opposite sides clamped (CFCF) are investigated. Here, 'C' and 'F' refer to clamped and free constraints. From Tables 6–8, it can be witnessed that the frequency decreases following the trend of CCCC > CCFF > CFCF. In addition, assessing the influence of skew angles and cut-out dimensions reveals that for CCFF condition, natural frequencies starts to deteriorate for skew angle $\lambda = 30^{o}$ and cut-out dimension of 0.6 m. Meanwhile, for CFCF condition the decreasing trend of natural frequency is noticed for $\lambda = 30^{o}$ and cut-out dimension of 0.4 m. The reason behind this variation trend can be attributed to the higher stiffness reduction with the increment in skew angle and cut-out dimension. In other words, the increment of skew angle results in increased length of skewed edges. In case of CCFF and CFCF boundary condition, there exist one and two free skewed edges, respectively. Therefore, the decreasing trend of frequency is noticed for 0.4 m itself for CFCF in contrast to CCFF. The mode shapes corresponding to the MEE plates with different boundary conditions, skew angles and cut-out dimensions are illustrated in Figs. (2)–(4).

2.3. Effect of coupling

The results shown in Tables 9–11 compare the effect of coupling fields on the fundamental natural frequency of MEE plate with various cut-out dimensions and skew angle. Here coupled state refers to complete interaction between magnetic and electric fields with the elastic field. Analogously, uncoupled state refers to influence of elastic field alone. From the results, it is revealed that for the

Table 5
Effect of cut-out on the natural frequency (in Hz) of square MEE plate (CCCC).

Mode Number	BFB				FBF			
	Cut-out dimension ($a_c = b_c$)							
	Without cut-out	0.3	0.4	0.5	Without cut-out	0.3	0.4	0.5
1	1594.4	1639.3	1999.9	2213.0	1656.2	1780.8	2386.3	2439.7
2	2012.3	2143.8	2572.5	2786.9	2478.1	2516.6	3019.9	3271.6
3	2123.7	2218.0	2661.6	2883.4	2444.9	2523.6	3028.4	3280.7

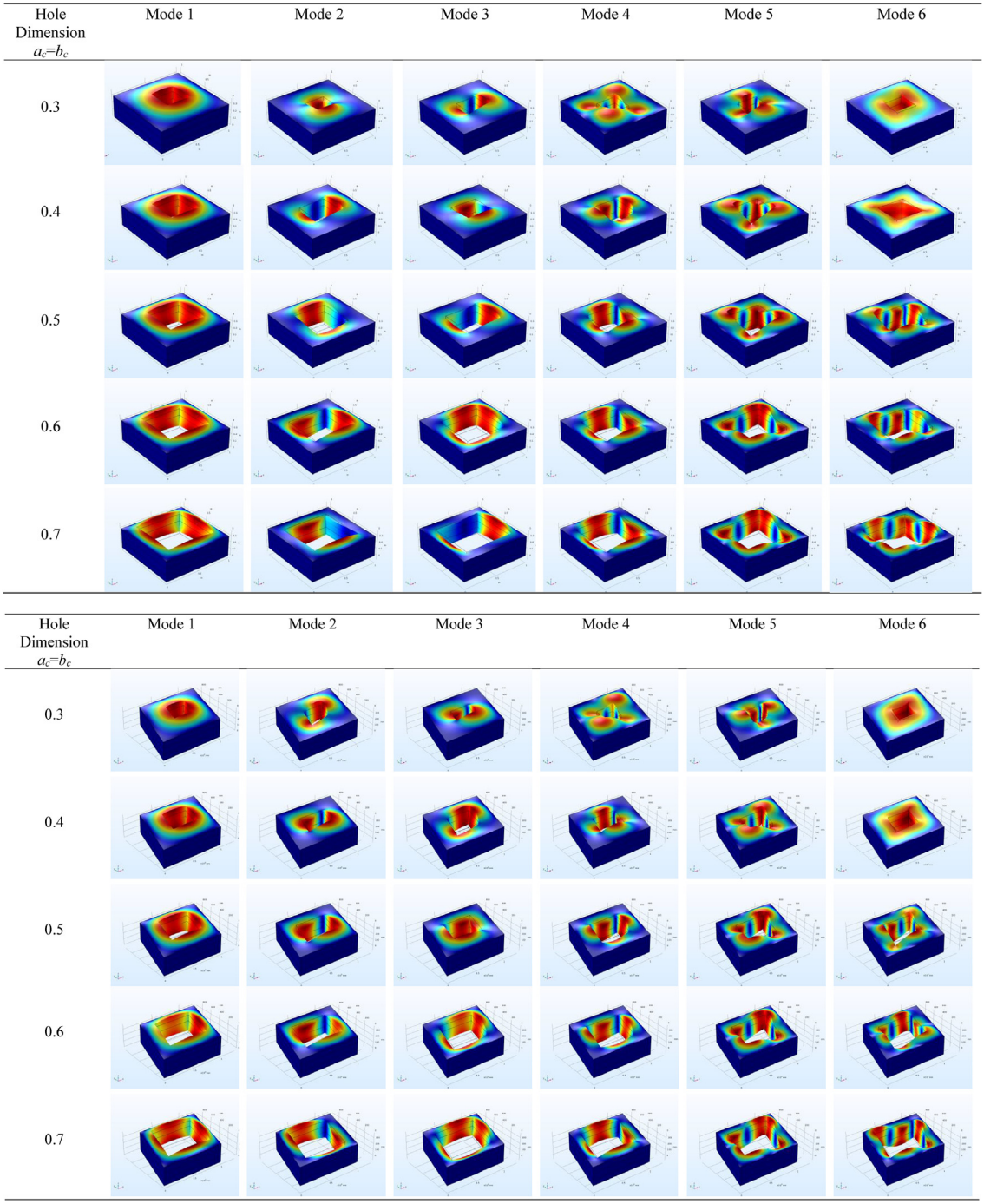

Fig. 2. a: First six mode shapes of MEE plate with different cut-out dimensions (CCCC$\lambda = 0^o$). Fig. 2b: First six mode shapes of MEE plate with different cut-out dimensions (CCCC $\lambda = 15^o$). Fig. 2c: First six mode shapes of MEE plate with different cut-out dimensions (CCCC$\lambda = 30^o$). Fig. 2d: First six mode shapes of MEE plate with different cut-out dimensions (CCCC $\lambda = 45^o$).

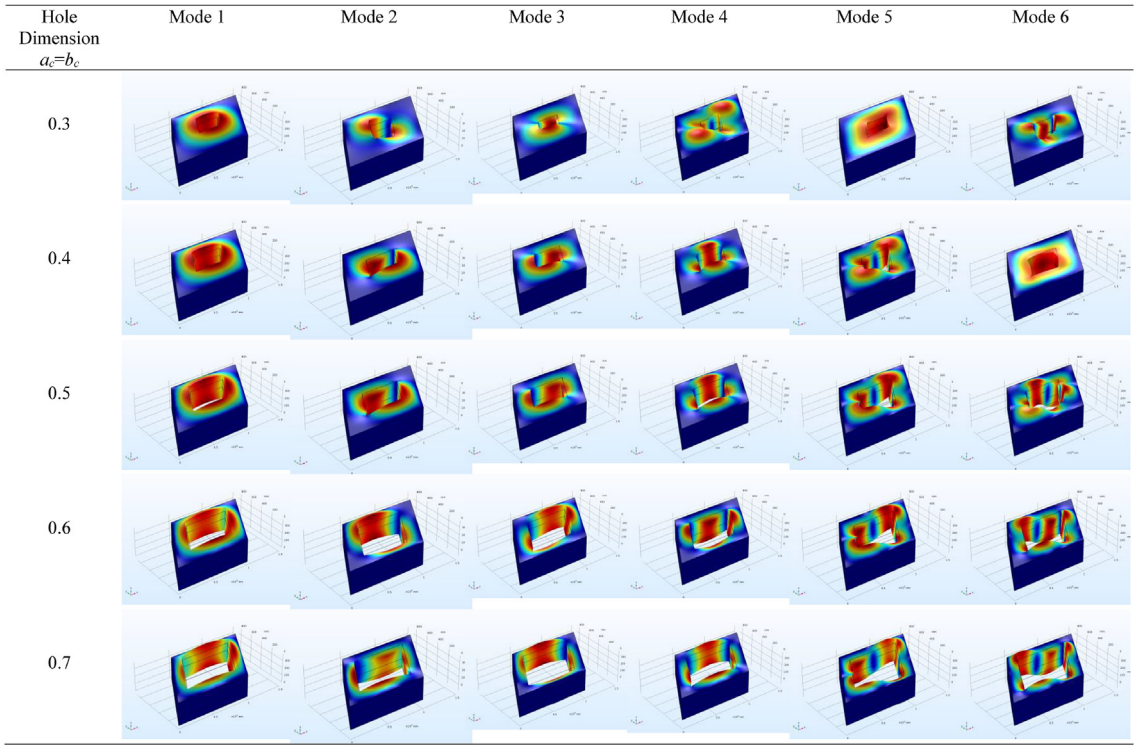

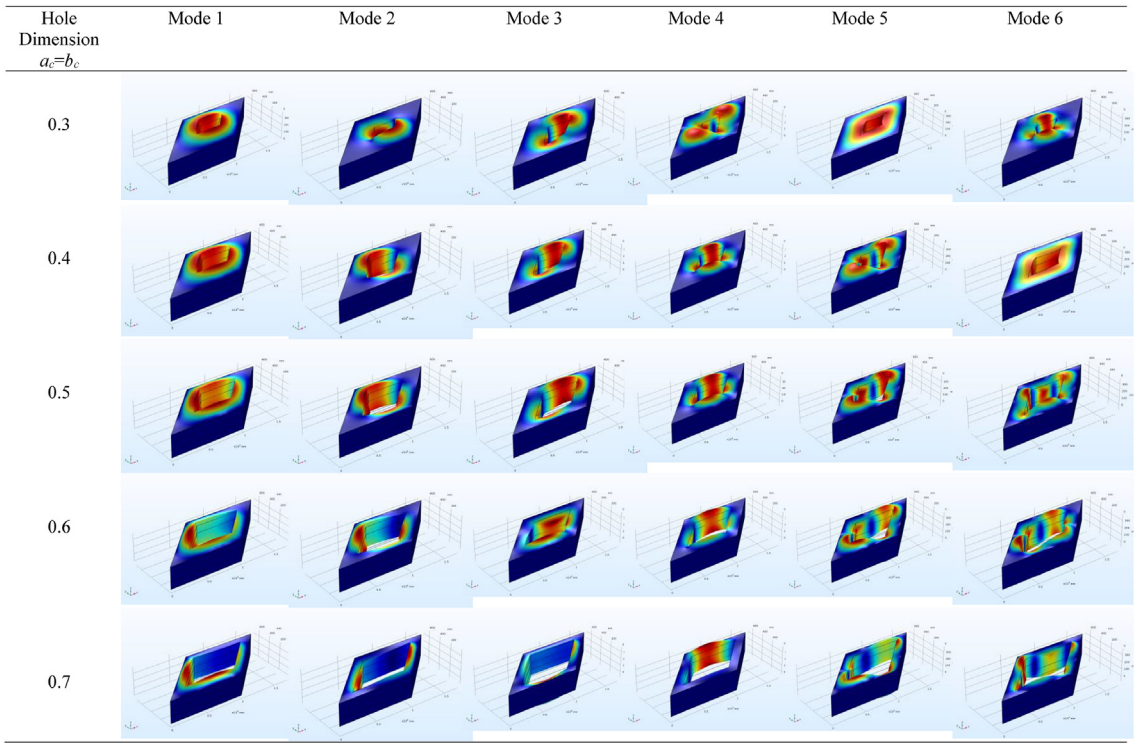

Fig. 2. (*continued*).

Table 6
Effect of skew angle and cut-out on the fundamental natural frequency (in Hz) of MEE plate with CCCC boundary condition.

Skew Angle (λ)	BFB					FBF				
	Cut-out dimension ($a_c = b_c$)									
	0.3	**0.4**	**0.5**	**0.6**	**0.7**	**0.3**	**0.4**	**0.5**	**0.6**	**0.7**
0	1639.3	1999.9	2213.0	2458.9	2635.6	1780.8	2386.3	2439.7	2528.7	2786.8
15	1711.3	2139.1	2344.4	2661.1	2749.7	1857.9	2452.4	2508.2	2656.8	3063.2
30	1950.1	2626.7	3057.8	3406.8	3987.9	1950.1	2652.1	2710.6	2827.7	2905.6
45	2468.8	3197.1	3508.2	4075.9	4932.6	2468.8	3777.2	3925.4	4048.8	4221.6

Table 7
Effect of skew angle and cut-out on the fundamental natural frequency (in Hz) of MEE plate skew angle with CCFF boundary condition.

Skew Angle (λ)	BFB					FBF				
	Cut-out dimension ($a_c = b_c$)									
	0.3	**0.4**	**0.5**	**0.6**	**0.7**	**0.3**	**0.4**	**0.5**	**0.6**	**0.7**
0	1475.4	1770.4	1888.5	1947.5	2006.5	1602.7	1987.4	2067.5	2163.7	2275.9
15	1540.2	1879.0	1940.6	2017.6	2125.4	1672.1	2023.3	2073.4	2190.5	2274.1
30	1755.1	2207.9	2587.0	**1983.6**	**1862.7**	1825.1	2211.4	2634.3	**2082.0**	**1992.2**
45	2221.9	**1910.7**	**1832.9**	**1768.4**	**1732.9**	2232.9	**2185.9**	**1991.8**	**1949.6**	**1844.0**

*The values in bold highlight the reduction in the frequency.

Table 8
Effect of skew angle and cut-out on the fundamental natural frequency (in Hz) of MEE plate with CFCF boundary condition.

Skew Angle (λ)	BFB					FBF				
	Cut-out dimension ($a_c = b_c$)									
	0.3	**0.4**	**0.5**	**0.6**	**0.7**	**0.3**	**0.4**	**0.5**	**0.6**	**0.7**
0	1362.4	1602.4	1686.0	1783.6	1839.3	1393.3	1662.0	1743.8	1811.9	1866.4
15	1421.7	1702.0	1789.2	1819.4	1876.1	1454.3	1741.8	1791.8	1847.3	1905.6
30	1657.6	**1595.7**	**1499.2**	**1443.5**	**1411.9**	1691.8	**1649.9**	**1559.5**	**1489.2**	**1434.0**
45	**1598.5**	**1512.9**	**1486.3**	**1406.0**	**1383.8**	**1618.6**	**1570.8**	**1511.9**	**1468.5**	**1394.7**

*The values in bold highlight the reduction in the frequency.

Table 9
Effect of coupling fields on the fundamental natural frequency (in Hz) of MEE plate with different skew angle and cut-out dimensions with CCCC boundary condition.

Cut-out dimension ($a_c = b_c$)	λ = 0°			λ = 15°			λ = 30°			λ = 45°		
	Coupled	Uncoupled	% Difference	Coupled	Uncoupled	% Difference	Coupled	Uncoupled	Difference	Coupled	Uncoupled	% Difference
	BFB											
0.3	1639.3	1604.87	2.1	1711.3	1658.24	3.1	1950.1	1862.34	4.5	2468.8	2288.57	7.3
0.4	1999.9	1947.70	2.6	2139.1	2066.37	3.4	2626.7	2492.73	5.1	3197.1	2934.93	8.2
0.5	2213.0	2142.18	3.2	2344.4	2255.31	3.8	3057.8	2855.9	6.6	3508.2	3052.13	**13.1**
0.6	2458.9	2301.53	**6.4**	2661.1	2461.51	**7.5**	3406.8	3066.12	**10.4**	4075.9	3464.51	**15.3**
0.7	2786.8	2555.41	**8.3**	3063.2	2784.43	**9.1**	3987.9	3493.40	**12.4**	4932.6	4143.33	**16.2**
FBF												
0.3	1780.8	1750.52	1.7	1857.9	1809.59	2.6	1950.1	1874.04	3.9	2498.8	2353.86	5.8
0.4	2386.3	2331.41	2.3	2452.4	2381.28	2.9	2452.4	2344.49	4.4	3777.2	3531.68	6.5
0.5	2439.7	2371.38	2.8	2508.2	2430.44	3.1	2508.2	2387.80	4.8	3925.4	3532.86	**10.1**
0.6	2528.7	2392.15	**5.4**	2656.8	2481.45	**6.6**	2656.8	2452.22	**7.7**	4048.8	3481.96	**14.8**
0.7	2635.6	2437.93	**7.5**	2749.7	2518.72	**8.4**	2749.7	2474.73	**10.3**	4221.6	3588.36	**15.4**

%difference= (Coupled-Uncoupled)/Uncoupled.
*The values in bold highlight the drastic change in the% difference.

Table 10
Effect of coupling fields on the fundamental natural frequency (in Hz) of MEE plate with different skew angle and cut-out dimensions with CCFF boundary condition.

Cut-out dimension ($a_c = b_c$)	$\lambda = 0^\circ$			$\lambda = 15^\circ$			$\lambda = 30^\circ$			$\lambda = 45^\circ$		
	Coupled	Uncoupled	% Difference	Coupled	Uncoupled	% Difference	Coupled	Uncoupled	Difference	Coupled	Uncoupled	% Difference
	BFB											
0.3	1475.4	1445.89	2.04	1540.2	1495.53	2.95	1755.1	1681.38	4.23	2221.9	2070.14	06.83
0.4	1770.4	1726.14	2.52	1879.0	1818.87	3.23	2207.9	2104.12	4.79	1910.7	1765.48	07.67
0.5	1888.5	1829.95	3.10	1940.6	1870.73	3.61	2587.0	2426.60	6.20	1832.9	1612.95	**12.26**
0.6	1947.5	1826.56	**6.21**	2017.6	1847.35	**7.13**	1983.6	1789.60	**9.78**	1768.4	1520.82	**14.31**
0.7	2006.5	1835.94	**8.05**	2125.4	1941.55	**8.65**	1862.7	1676.43	**11.66**	1732.9	1472.96	**15.16**
FBF												
0.3	1602.7	1577.056	1.60	1672.1	1631.96	2.47	1825.1	1759.39	3.63	2232.9	2119.02	05.12
0.4	1987.4	1945.66	2.17	2023.3	1968.67	2.76	2211.4	2122.94	4.09	2185.9	2061.30	05.73
0.5	2067.5	2013.74	2.64	2073.4	2013.27	2.95	2634.3	2513.12	4.46	1991.8	1814.52	**08.90**
0.6	2163.7	2053.35	**5.10**	2190.5	2054.68	**6.27**	2082.0	1934.17	**7.16**	1949.6	1696.15	**13.05**
0.7	2275.9	2116.58	**7.08**	2274.1	2094.44	**7.98**	1992.2	1802.94	**9.58**	1844.0	1604.28	**13.57**

%difference= (Coupled-Uncoupled)/Uncoupled.
*The values in bold highlight the drastic change in the% difference.

Table 11
Effect of coupling fields on the fundamental natural frequency (in Hz) of MEE plate with different skew angle and cut-out dimensions with CFCF boundary condition.

Cut-out dimension ($a_c = b_c$)	$\lambda = 0^\circ$			$\lambda = 15^\circ$			$\lambda = 30^\circ$			$\lambda = 45^\circ$		
	Coupled	Uncoupled	% Difference	Coupled	Uncoupled	% Difference	Coupled	Uncoupled	Difference	Coupled	Uncoupled	% Difference
	BFB											
0.3	1362.4	1335.8	1.95	1421.7	1380.6	2.89	1657.6	1590.6	4.04	1598.5	1497.6	6.31
0.4	1602.4	1563.8	2.41	1702.0	1648.1	3.17	1595.7	1522.8	4.57	1512.9	1405.8	7.08
0.5	1686.0	1635.9	2.97	1789.2	1725.9	3.54	1499.2	1410.4	5.92	1486.3	1318.1	**11.32**
0.6	1783.6	1677.6	**5.94**	1819.4	1692.2	**6.99**	1443.5	1308.8	**9.33**	1406.0	1220.3	**13.21**
0.7	1839.3	1697.7	**7.70**	1876.1	1717.0	**8.48**	1411.9	1254.8	**11.13**	1383.8	1190.1	**14.00**
FBF												
0.3	1393.3	1371.84	1.54	1453.3	1418.3	2.41	1691.8	1633.1	3.47	1618.6	1443.8	10.8
0.4	1662.0	1627.26	2.09	1741.8	1694.9	2.69	1649.9	1585.4	3.91	1570.8	1388.6	11.6
0.5	1743.8	1699.33	2.55	1791.8	1740.2	2.88	1559.5	1492.9	4.27	1511.9	1324.4	**12.4**
0.6	1811.9	1722.75	**4.92**	1847.3	1734.3	**6.12**	1489.2	1387.2	**6.85**	1468.5	1270.3	**13.5**
0.7	1866.4	1738.74	**6.84**	1905.6	1757.3	**7.78**	1434.0	1302.7	**9.16**	1394.7	1195.3	**14.3**

%difference= (Coupled-Uncoupled)/Uncoupled.
*The values in bold highlight the drastic change in the% difference.

given cut-out dimension, with the increase in skew angle the discrepancy between the coupled and uncoupled frequency improves. On the other hand, for a given skew angle, as the cut-out dimension increases higher coupling effect is noticed. However, it can be witnessed that with cut-out dimension more than 0.5 m, the percentage difference drastically increases. This may be attributed to the fact that the stiffness of the MEE plate reduces and its contribution to the $[K_{eq}]$ (coupled stiffness) also reduces. Further, among all the boundary conditions considered for evaluation, a predominant influence (in terms of % difference) of all sides clamped (CCCC) is noticed. This is due to the higher stiffness provided by CCCC condition.

3. Conclusions

This article addresses the coupled frequency analysis of MEE plate with cut-outs using FE methods for the first time. Using Hamilton's principle the governing equations of motion are derived. The credibility of the proposed formulation is verified by comparing the results with the previously published literature as well as with the numerical software. The results reveal that for CCCC condition, the frequency improves with higher cut-out dimension. However, for CCFF and CFCF condition after certain limit of the cut-out dimension and the skew angle the frequency tends to decrease. Further, evaluation on the influence of coupling

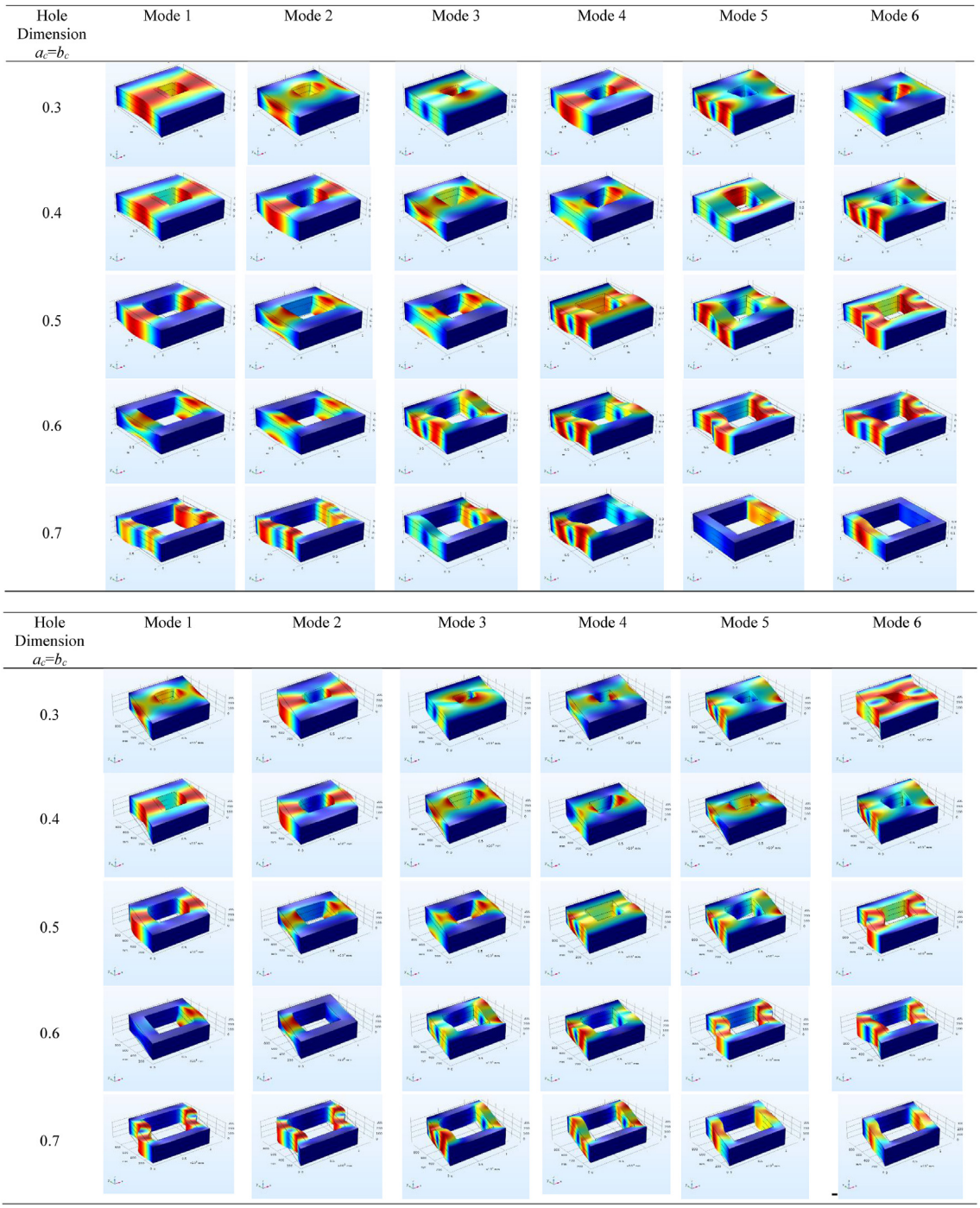

Fig. 3. a: First six mode shapes of MEE plate with different cut-out dimensions (CFCF $\lambda = 0^o$). Fig. 3b: First six mode shapes of MEE plate with different cut-out dimensions (CFCF; $\lambda = 15^o$). Fig. 3c: First six mode shapes of MEE plate with different cut-out dimensions (CFCF; $\lambda = 30^o$). Fig. 3d: First six mode shapes of MEE plate with different cut-out dimensions (CFCF; $\lambda = 45^o$).

fields suggest that for higher cut-out dimension (say 0.5 m and above) the effect becomes very predominant. It is believed that the results of this article may act as benchmark solutions for further researches on MEE smart structures.

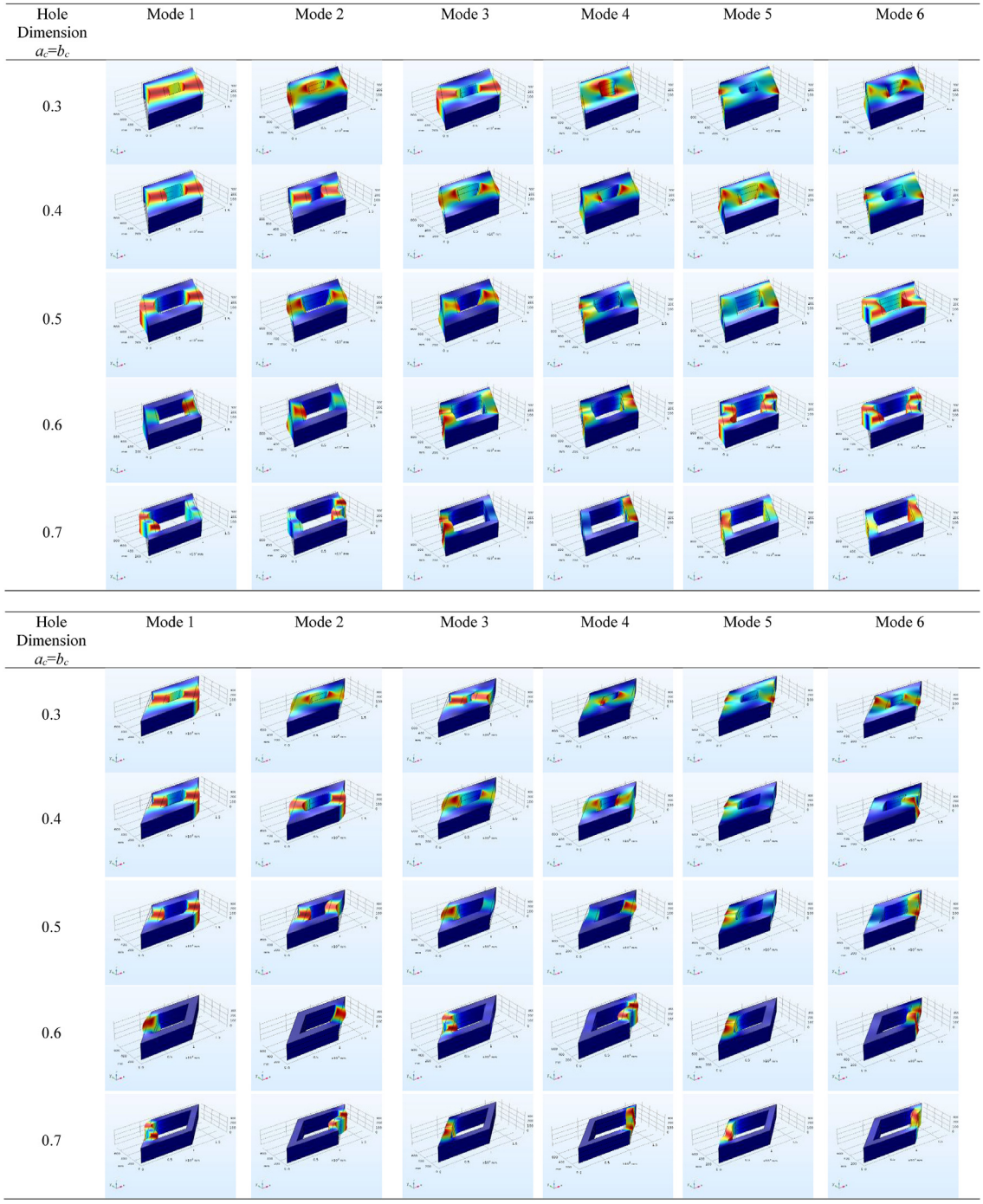

Fig. 3. (*continued*).

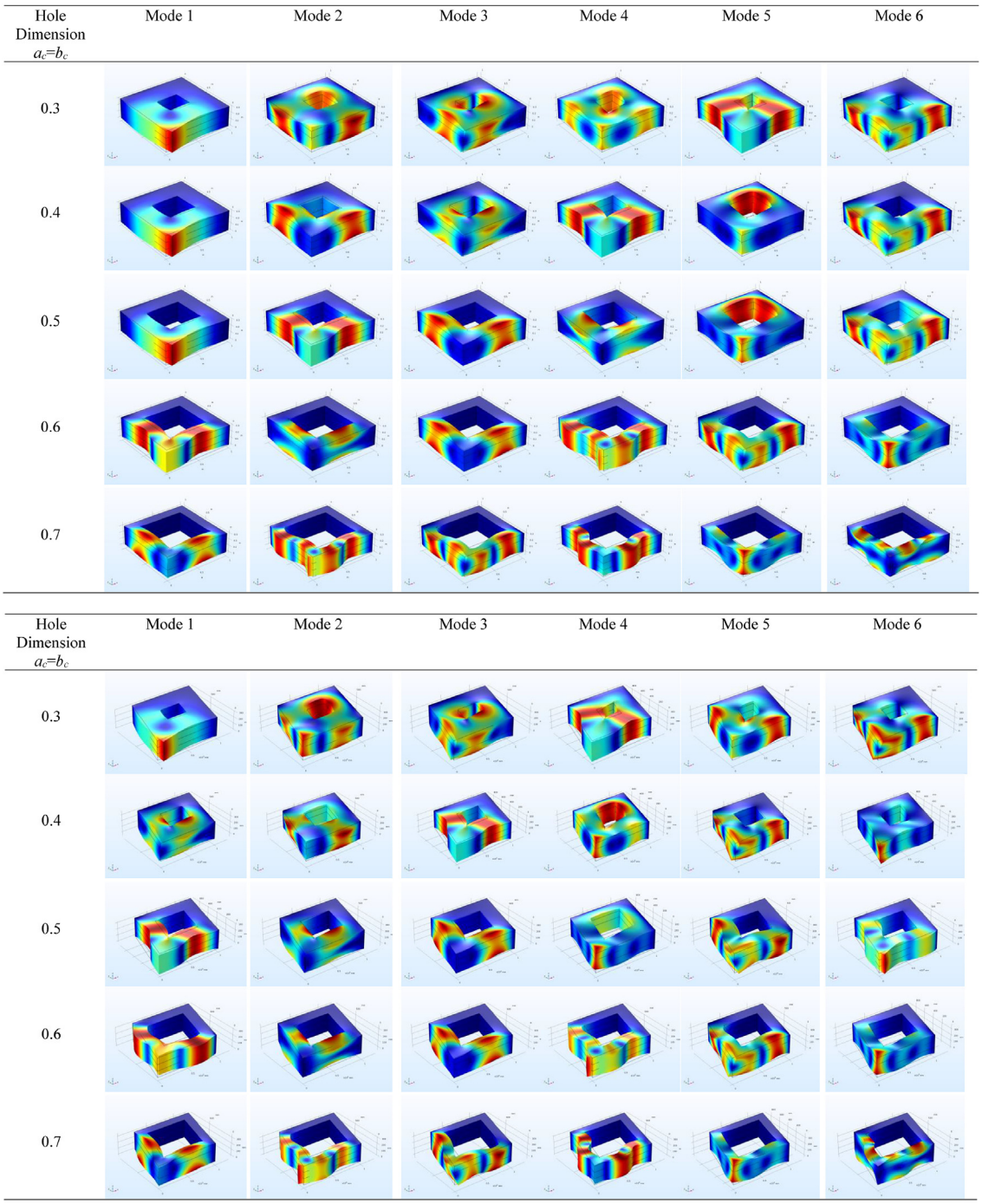

Fig. 4. a: First six mode shapes of MEE plate with different cut-out dimensions (CCFF; $\lambda = 0^o$). Fig. 4b: First six mode shapes of MEE plate with different cut-out dimensions (CCFF $\lambda = 15^o$). Fig. 4c: First six mode shapes of MEE plate with different cut-out dimensions (CCFF; $\lambda = 30^o$). Fig. 4d: First six mode shapes of MEE plate with different cut-out dimensions (CCFF; $\lambda = 45^o$).

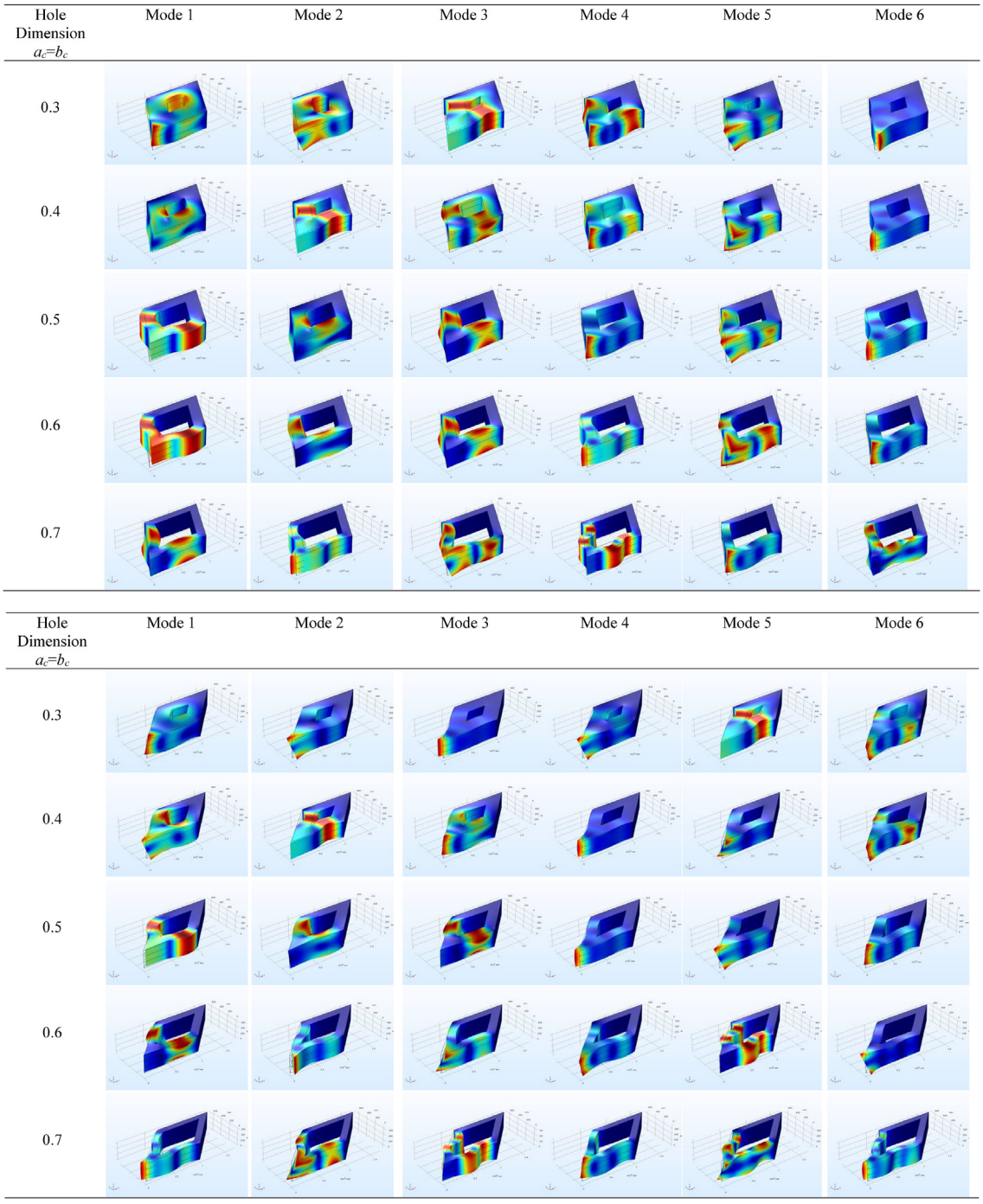

Fig. 4. (*continued*).

4. Data availability

The raw/processed data required to reproduce these findings cannot be shared at this time as the data also forms part of an ongoing study.

Declaration of competing interest

I have the pleasure of sending you the manuscript entitled **"A higher order coupled frequency characteristics study of smart magneto-electro-elastic composite plates with cut-outs using finite element methods"** to be considered for publication as a research article in your prestigious journal **Defence Technology.**

Acknowledgements

The first author acknowledges the support of Indian Institute of Science, Bangalore, through C.V. Raman Post-doctoral fellowship, under Institution of Eminence scheme.

Appendix

The constitutive equations of transversely isotropic MEE material MEE materials can be represented as follows [35]:

$$\begin{aligned}\{\sigma\} &= [\tilde{C}]\{\varepsilon\} - [\tilde{e}]\{E\} - [\tilde{q}]\{H\}\\ \{D\} &= [\tilde{e}]^T\{\varepsilon\} - [\tilde{\eta}]\{E\} - [\tilde{m}]\{H\}\\ \{B\} &= [\tilde{q}]^T\{\varepsilon\} - [\tilde{m}]\{E\} - [\tilde{\mu}]\{H\}\end{aligned} \tag{A-1}$$

where $[\tilde{C}]$, $[\tilde{e}]$ and $[\tilde{q}]$ are the reduced elastic stiffness co-efficient, the piezoelectric coefficient and the magnetostrictive coefficient matrices respectively; $[\tilde{\eta}]$, $[\tilde{m}]$ and $[\tilde{\mu}]$ are the reduced dielectric coefficient, electromagnetic coefficient and the magnetic permeability coefficient matrices respectively; $\{\sigma\}$, $\{D\}$ and $\{B\}$, represent the stress tensor, electric displacement and the magnetic flux, respectively; $\{\varepsilon\}$, $\{E\}$ and $\{H\}$ are the linear strain tensor, electric field and magnetic field, respectively.

The different shape function matrices appearing in Eq. (2) can be summarized as follows:

$$\begin{aligned}[N_t] &= \begin{bmatrix} N_1 & 0 & 0 & N_2 & 0 & 0 & N_8 & 0 & 0\\ 0 & N_1 & 0 & 0 & N_2 & 0 & \cdots\ 0 & N_8 & 0\\ 0 & 0 & N_1 & 0 & 0 & N_2 & 0 & 0 & N_8 \end{bmatrix},\ [N_r] = [N_{r*}]\\ &= \begin{bmatrix} N_1 & 0 & N_2 & 0 & \cdots & N_8 & 0\\ 0 & N_1 & 0 & N_2 & & 0 & N_8 \end{bmatrix},\ [N_\varphi] = [N_\psi] = [N_1\ N_2 \cdots N_8]\end{aligned} \tag{A-2}$$

The various strain-displacement matrices appearing in Eq. (3) can be expressed as follows:

$$\begin{aligned}[B_{tb}] &= \begin{bmatrix} N_{i,x} & 0 & 0\\ 0 & N_{i,y} & 0\\ N_{i,y} & N_{i,x} & 0 \end{bmatrix},\ [B_{rb}] = \begin{bmatrix} N_{i,x} & 0\\ 0 & N_{i,y}\\ N_{i,y} & N_{i,x} \end{bmatrix}\\ [B_{ts}] &= \begin{bmatrix} 0 & 0 & N_{i,x}\\ 0 & 0 & N_{i,y} \end{bmatrix},\ [B_{rs}] = \begin{bmatrix} 1 & 0\\ 0 & 1 \end{bmatrix}\end{aligned} \tag{A-3}$$

Incorporating the constitutive equations (Eq. (A-1)), finite element parameters (Eqs. (1)–(4) and Eqs. (6) and (7)) in the Hamilton's principle (Eq. (5)), the equations of motion are arrived in a manner as follows:

$$\frac{1}{2}\sum_{n=1}^{N}\delta\int_{\Omega_p^n}\left(\{d_{r*}^e\}^T[B_{rb}]^T c_1 z^3 + \{d_r^e\}^T[B_{rb}]^T c_1 z^3 + \{d_r^e\}^T[B_{rb}]^T z + \{d_t^e\}^T[B_{tb}]^T\right)*$$

$$\left\{\begin{array}{l}\left([C_b][B_{tb}]\{d_t^e\} + z[C_b][B_{rb}]\{d_r^e\} + c_1 z^3[C_b][B_{rb}]\{d_r^e\} + c_1 z^3[C_b][B_{rb}]\{d_{r*}^e\}\right)\\ -\{e\}[E] - \{q\}[H]\end{array}\right\}\Omega_p^n$$

$$-\frac{1}{2}\sum_{n=1}^{N}\delta\int_{\Omega_h^n}\left(\{d_{r*}^e\}^T[B_{rb}]^T c_1 z^3 + \{d_r^e\}^T[B_{rb}]^T c_1 z^3 + \{d_r^e\}^T[B_{rb}]^T z + \{d_t^e\}^T[B_{tb}]^T\right)*$$

$$\left\{\begin{array}{l}\left([C_b][B_{tb}]\{d_t^e\} + z[C_b][B_{rb}]\{d_r^e\} + c_1 z^3[C_b][B_{rb}]\{d_r^e\} + c_1 z^3[C_b][B_{rb}]\{d_{r*}^e\}\right)\\ -\{e\}[E] - \{q\}[H]\end{array}\right\}\Omega_h^n$$

$$+\frac{1}{2}\sum_{n=1}^{N}\delta\int_{\Omega_p^n}\left(\{d_{r*}^e\}^T[B_{rs}]^T c_2 z^2 + \{d_r^e\}^T[B_{rs}]^T c_2 z^2 + \{d_r^e\}^T[B_{rs}]^T + \{d_t^e\}^T[B_{ts}]^T\right)*$$

$$\left\{\begin{pmatrix}[C_s][B_{ts}]\{d_t^e\} + z[C_s][B_{rs}]\{d_r^e\} + c_2 z^2[C_s][B_{rs}]\{d_r^e\} + c_2 z^2[C_s][B_{rs}]\{d_{r*}^e\}\\ -[e][E] - [q][H]\end{pmatrix}\right\}\Omega_p^n$$

$$-\frac{1}{2}\sum_{n=1}^{N}\delta\int_{\Omega_h^n}\left(\{d_{r*}^e\}^T[B_{rs}]^T c_2 z^2 + \{d_r^e\}^T[B_{rs}]^T c_2 z^2 + \{d_r^e\}^T[B_{rs}]^T + \{d_t^e\}^T[B_{ts}]^T\right)*$$

$$\left\{\begin{pmatrix}[C_s][B_{ts}]\{d_t^e\} + z[C_s][B_{rs}]\{d_r^e\} + c_2 z^2[C_s][B_{rs}]\{d_r^e\} + c_2 z^2[C_s][B_{rs}]\{d_{r*}^e\}\\ -[e][E] - [q][H]\end{pmatrix}\right\}\Omega_h^n$$

$$-\frac{1}{2}\sum_{n=1}^{N}\delta\int_{\Omega_p^n}\begin{bmatrix}\{\varphi\}^T[B_\varphi]^T[e_b]^T[B_{tb}]\{d_t^e\}+\{\varphi\}^T[B_\varphi]^T[e_b]^Tz[B_{rb}]\{d_r^e\}+\{\varphi\}^T[B_\varphi]^T[e_b]^Tc_1z^3[B_{rb}]\{d_r^e\}+\\ \{\varphi\}^T[B_\varphi]^T[e_b]^Tc_1z^3[B_{rb}]\{d_{r*}^e\}+\{\varphi\}^T[B_\varphi]^T[e_s]^T[B_{ts}]\{d_t^e\}+\{\varphi\}^T[B_\varphi]^T[e_s]^T[B_{rs}]\{d_r^e\}+\\ \{\varphi\}^T[B_\varphi]^T[e_s]^Tc_2z^2[B_{rs}]\{d_r^e\}+\{\varphi\}^T[B_\varphi]^T[e_s]^Tc_2z^2[B_{rs}]\{d_{r*}^e\}+\{\varphi\}^T[B_\varphi]^T[\eta][B_\varphi]\{\varphi\}+\\ \{\varphi\}^T[B_\varphi]^T[m][B_\psi]\{\psi\}\end{bmatrix}$$

$$-\frac{1}{2}\sum_{n=1}^{N}\delta\int_{\Omega_h^n}\begin{bmatrix}\{\varphi\}^T[B_\varphi]^T[e_b]^T[B_{tb}]\{d_t^e\}+\{\varphi\}^T[B_\varphi]^T[e_b]^Tz[B_{rb}]\{d_r^e\}+\{\varphi\}^T[B_\varphi]^T[e_b]^Tc_1z^3[B_{rb}]\{d_r^e\}+\\ \{\varphi\}^T[B_\varphi]^T[e_b]^Tc_1z^3[B_{rb}]\{d_{r*}^e\}+\{\varphi\}^T[B_\varphi]^T[e_s]^T[B_{ts}]\{d_t^e\}+\{\varphi\}^T[B_\varphi]^T[e_s]^T[B_{rs}]\{d_r^e\}+\\ \{\varphi\}^T[B_\varphi]^T[e_s]^Tc_2z^2[B_{rs}]\{d_r^e\}+\{\varphi\}^T[B_\varphi]^T[e_s]^Tc_2z^2[B_{rs}]\{d_{r*}^e\}+\{\varphi\}^T[B_\varphi]^T[\eta][B_\varphi]\{\varphi\}+\\ \{\varphi\}^T[B_\varphi]^T[m][B_\psi]\{\psi\}\end{bmatrix}$$

$$-\frac{1}{2}\sum_{n=1}^{N}\delta\int_{\Omega_p^n}\begin{bmatrix}\{\psi\}^T[B_\psi]^T[q_b]^T[B_{tb}]\{d_t^e\}+\{\psi\}^T[B_\psi]^T[q_b]^Tz[B_{rb}]\{d_r^e\}+\{\psi\}^T[B_\psi]^T[q_b]^Tc_1z^3[B_{rb}]\{d_r^e\}+\\ \{\psi\}^T[B_\psi]^T[q_b]^Tc_1z^3[B_{rb}]\{d_{r*}^e\}+\{\psi\}^T[B_\psi]^T[q_s]^T[B_{ts}]\{d_t^e\}+\{\psi\}^T[B_\psi]^T[q_s]^T[B_{rs}]\{d_r^e\}+\\ \{\psi\}^T[B_\psi]^T[q_s]^Tc_2z^2[B_{rs}]\{d_r^e\}+\{\psi\}^T[B_\psi]^T[q_s]^Tc_2z^2[B_{rs}]\{d_{r*}^e\}+\{\psi\}^T[B_\psi]^T[m][B_\varphi]\{\varphi\}+\\ \{\psi\}^T[B_\psi]^T[\mu][B_\psi]\{\psi\}\end{bmatrix}$$

$$-\frac{1}{2}\sum_{n=1}^{N}\delta\int_{\Omega_h^n}\begin{bmatrix}\{\psi\}^T[B_\psi]^T[q_b]^T[B_{tb}]\{d_t^e\}+\{\psi\}^T[B_\psi]^T[q_b]^Tz[B_{rb}]\{d_r^e\}+\{\psi\}^T[B_\psi]^T[q_b]^Tc_1z^3[B_{rb}]\{d_r^e\}+\\ \{\psi\}^T[B_\psi]^T[q_b]^Tc_1z^3[B_{rb}]\{d_{r*}^e\}+\{\psi\}^T[B_\psi]^T[q_s]^T[B_{ts}]\{d_t^e\}+\{\psi\}^T[B_\psi]^T[q_s]^T[B_{rs}]\{d_r^e\}+\\ \{\psi\}^T[B_\psi]^T[q_s]^Tc_2z^2[B_{rs}]\{d_r^e\}+\{\psi\}^T[B_\psi]^T[q_s]^Tc_2z^2[B_{rs}]\{d_{r*}^e\}+\{\psi\}^T[B_\psi]^T[m][B_\varphi]\{\varphi\}+\\ \{\psi\}^T[B_\psi]^T[\mu][B_\psi]\{\psi\}\end{bmatrix}$$

$$+\left[\left[M^e_{tt\_p}\right]-\left[M^e_{tt\_h}\right]\right]\{\ddot{d}^e_t\}=0 \tag{A-4}$$

Bifurcating the terms based on the coefficients of $\{d^e_t\}^T$, $\{d^e_r\}^T$, $\{d^e_{r*}\}^T$, $\{\varphi^e\}^T$ and $\{\psi^e\}^T$ and applying condensation procedure [35], the global equations of motion of MEE plate with cut-out can be represented in the form as follows:

$$\begin{aligned}
&[M_{tt}]\{\ddot{d}_t\}+[K_{tt}]\{d_t\}+[K_{tr}]\{d_r\}+[K_{tr*}]\{d_{r*}\}+[K_{t\varphi}]\{\varphi\}\\
&\quad+[K_{t\psi}]\{\psi\}\\
&=0[K_{rt}]\{d_t\}+[K_{rr}]\{d_r\}+[K_{rr*}]\{d_{r*}\}+[K_{r\varphi}]\{\varphi\}+[K_{r\psi}]\{\psi\}\\
&=0[K_{r*t}]\{d_t\}+[K_{r*r}]\{d_r\}+[K_{r*r*}]\{d_{r*}\}+[K_{r*\varphi}]\{\varphi\}\\
&\quad+[K_{r*\psi}]\{\psi\}\\
&=0[K_{\varphi t}]\{d_t\}+[K_{\varphi r}]\{d_r\}+[K_{\varphi r*}]\{d_{r*}\}+[K_{\varphi\varphi}]\{\varphi\}+[K_{\varphi\psi}]\{\psi\}\\
&=0[K_{\psi t}]\{d_t\}+[K_{\psi r}]\{d_r\}+[K_{\psi r*}]\{d_{r*}\}+[K_{\psi\varphi}]\{\varphi\}+[K_{\psi\psi}]\{\psi\}\\
&=0
\end{aligned} \tag{A-5}$$

The various elemental stiffness matrices contributing to the equations of motion are as follows:

Each stiffness matrix can be explicitly represented as follows:

$$\left[K^e_{\psi\psi\_p}\right]=\int_0^a\int_0^b[B_\psi]^T[D_{\psi\psi}][B_\psi]\;dx\,dy,$$

$$\left[K^e_{\psi\psi\_h}\right]=\int_0^{a_c}\int_0^{b_c}[B_\psi]^T[D_{\psi\psi}][B_\psi]\;dx\,dy,$$

$$\left[K^e_{\varphi\varphi\_p}\right]=\int_0^a\int_0^b[B_\varphi]^T[D_{\varphi\varphi}][B_\varphi]\;dx\,dy,$$

$$\left[K^e_{\varphi\varphi\_h}\right]=\int_0^{a_c}\int_0^{b_c}[B_\varphi]^T[D_{\varphi\varphi}][B_\varphi]\;dx\,dy,$$

$$\begin{aligned}
&[K^e_{tt}]=\left[K^e_{tb1_p}\right]-\left[K^e_{tb1_h}\right]+\left[K^e_{ts1_p}\right]-\left[K^e_{ts1_h}\right],\ [K^e_{tr}]=\left[K^e_{rtb24_p}\right]^T-\left[K^e_{rtb24_h}\right]^T+\left[K^e_{rts13_p}\right]^T-\left[K^e_{rts13_h}\right]^T\\
&[K^e_{tr*}]=\left[K^e_{rtb4_p}\right]^T-\left[K^e_{rtb4_h}\right]^T+\left[K^e_{rts3_p}\right]^T-\left[K^e_{rts3_h}\right]^T,\ [K^e_{t\varphi}]=\left[K^e_{tb\varphi1_p}\right]-\left[K^e_{tb\varphi1_h}\right]+\left[K^e_{ts\varphi1_p}\right]-\left[K^e_{ts\varphi1_h}\right]\\
&[K^e_{t\psi}]=\left[K^e_{tb\psi1_p}\right]-\left[K^e_{tb\psi1_h}\right]+\left[K^e_{ts\psi1_p}\right]-\left[K^e_{ts\psi1_h}\right],\ [K^e_{rr}]=\left[K^e_{rrb5735_p}\right]-\left[K^e_{rrb5735_h}\right]+\left[K^e_{rrs3513_p}\right]-\left[K^e_{rrs3513_h}\right]\\
&[K^e_{rr*}]=\left[K^e_{rrb57_p}\right]-\left[K^e_{rrb57_h}\right]+\left[K^e_{rrs35_p}\right]-\left[K^e_{rrs35_h}\right],\ [K^e_{r\varphi}]=\left[K^e_{rb\varphi24_p}\right]-\left[K^e_{rb\varphi24_h}\right]+\left[K^e_{r\varphi s13_p}\right]-\left[K^e_{r\varphi s13_h}\right]\\
&[K^e_{r\psi}]=\left[K^e_{rb\psi24_p}\right]-\left[K^e_{rb\psi24_h}\right]+\left[K^e_{r\psi s13_p}\right]-\left[K^e_{r\psi s13_h}\right],\ [K^e_{r*r*}]=\left[K^e_{rrb7_p}\right]+\left[K^e_{rrs5_p}\right]-\left[K^e_{rrb7_h}\right]-\left[K^e_{rrs5_h}\right]\\
&[K^e_{r*\varphi}]=\left[K^e_{rb\varphi4_p}\right]-\left[K^e_{rb\varphi4_h}\right]+\left[K^e_{r\varphi s3_p}\right]-\left[K^e_{r\varphi s3_h}\right]\\
&[K^e_{r*\psi}]=\left[K^e_{rb\psi4_p}\right]+\left[K^e_{r\psi s3_p}\right]-\left[K^e_{rb\psi4_h}\right]-\left[K^e_{r\psi s3_h}\right],\ [K^e_{rrt}]=\left[K^e_{rtb24_p}\right]+\left[K^e_{rts13_p}\right]-\left[K^e_{rtb24_h}\right]-\left[K^e_{rts13_h}\right]\\
&[K^e_{rrb5735}]=\left[K^e_{rrb57_p}\right]+\left[K^e_{rrb35_p}\right]-\left[K^e_{rrb57_h}\right]-\left[K^e_{rrb35_h}\right],\ [K^e_{rrs3513}]=\left[K^e_{rrs35_p}\right]+\left[K^e_{rrs13_p}\right]-\left[K^e_{rrs35_h}\right]-\left[K^e_{rrs13_h}\right]\\
&[K^e_{rrb57}]=\left[K^e_{rrb5_p}\right]+\left[K^e_{rrb7_p}\right]-\left[K^e_{rrb5_h}\right]-\left[K^e_{rrb7_h}\right],\ [K^e_{rrb35}]=\left[K^e_{rrb3_p}\right]+\left[K^e_{rrb5_p}\right]-\left[K^e_{rrb3_h}\right]-\left[K^e_{rrb5_h}\right]\\
&[K^e_{rrs35}]=\left[K^e_{rrs3_p}\right]+\left[K^e_{rrs5_p}\right]-\left[K^e_{rrs3_h}\right]-\left[K^e_{rrs5_h}\right],\ [K^e_{rrs13}]=\left[K^e_{rrs1_p}\right]+\left[K^e_{rrs3_p}\right]-\left[K^e_{rrs1_h}\right]-\left[K^e_{rrs3_h}\right]\\
&[K^e_{rb\varphi24}]=\left[K^e_{rb\varphi2_p}\right]+\left[K^e_{rb\varphi4_p}\right]-\left[K^e_{rb\varphi2_h}\right]-\left[K^e_{rb\varphi4_h}\right],\ [K^e_{r\varphi s13}]=\left[K^e_{r\varphi s1_p}\right]+\left[K^e_{r\varphi s3_p}\right]-\left[K^e_{r\varphi s1_h}\right]-\left[K^e_{r\varphi s3_h}\right]\\
&[K^e_{rb\psi24}]=\left[K^e_{rb\psi2_p}\right]+\left[K^e_{rb\psi4_p}\right]-\left[K^e_{rb\psi2_h}\right]-\left[K^e_{rb\psi4_h}\right],\ [K^e_{r\psi s13}]=\left[K^e_{r\psi s1_p}\right]+\left[K^e_{r\psi s3_p}\right]-\left[K^e_{r\psi s1_h}\right]-\left[K^e_{r\psi s3_h}\right]
\end{aligned} \tag{A-6}$$

$$\left[K^e_{tb1\_p}\right] = \int_0^a \int_0^b [B_{tb}]^T [D_{b1}][B_{tb}]\ dxdy,$$

$$\left[K^e_{tb1\_h}\right] = \int_0^{a_c} \int_0^{b_c} [B_{tb}]^T [D_{b1}][B_{tb}]\ dxdy,$$

$$\left[K^e_{ts1\_p}\right] = \int_0^a \int_0^b [B_{ts}]^T [D_{s1}][B_{ts}]\ dxdy,$$

$$\left[K^e_{ts1\_h}\right] = \int_0^{a_c} \int_0^{b_c} [B_{ts}]^T [D_{s1}][B_{ts}]\ dxdy,$$

$$\left[K^e_{rtb4\_p}\right] = \int_0^a \int_0^b [B_{rb}]^T [D_{b4}][B_{tb}]\ dxdy,$$

$$\left[K^e_{rtb4\_h}\right] = \int_0^{a_c} \int_0^{b_c} [B_{rb}]^T [D_{b4}][B_{tb}]\ dxdy,$$

$$\left[K^e_{rts3\_p}\right] = \int_0^a \int_0^b [B_{rs}]^T [D_{s3}][B_{ts}]\ dxdy,$$

$$\left[K^e_{rts3\_h}\right] = \int_0^{a_c} \int_0^{b_c} [B_{rs}]^T [D_{s3}][B_{ts}]\ dxdy,$$

$$\left[K^e_{tb\varphi1\_p}\right] = \int_0^a \int_0^b [B_{tb}]^T [D_{b\varphi1}][B_{\varphi}]\ dxdy,$$

$$\left[K^e_{tb\varphi1\_h}\right] = \int_0^{a_c} \int_0^{b_c} [B_{tb}]^T [D_{b\varphi1}][B_{\varphi}]\ dxdy,$$

$$\left[K^e_{ts\varphi1\_p}\right] = \int_0^a \int_0^b [B_{ts}]^T [D_{s\varphi1}][B_{\varphi}]\ dxdy,$$

$$\left[K^e_{ts\varphi1\_h}\right] = \int_0^{a_c} \int_0^{b_c} [B_{ts}]^T [D_{s\varphi1}][B_{\varphi}]\ dxdy,$$

$$\left[K^e_{tb\psi1\_p}\right] = \int_0^a \int_0^b [B_{tb}]^T [D_{b\psi1}][B_{\psi}]\ dxdy,$$

$$\left[K^e_{tb\psi1\_h}\right] = \int_0^{a_c} \int_0^{b_c} [B_{tb}]^T [D_{b\psi1}][B_{\psi}]\ dxdy,$$

$$\left[K^e_{ts\psi1\_p}\right] = \int_0^a \int_0^b [B_{ts}]^T [D_{s\psi1}][B_{\psi}]\ dxdy,$$

$$\left[K^e_{ts\psi1\_h}\right] = \int_0^{a_c} \int_0^{b_c} [B_{ts}]^T [D_{s\psi1}][B_{\psi}]\ dxdy,$$

$$\left[K^e_{rrb7\_p}\right] = \int_0^a \int_0^b [B_{rb}]^T [D_{b7}][B_{rb}]\ dxdy,$$

$$\left[K^e_{rrb7\_h}\right] = \int_0^{a_c} \int_0^{b_c} [B_{rb}]^T [D_{b7}][B_{rb}]\ dxdy,$$

$$\left[K^e_{rrs5\_p}\right] = \int_0^a \int_0^b [B_{rs}]^T [D_{s5}][B_{rs}]\ dxdy,$$

$$\left[K^e_{rrs5\_h}\right] = \int_0^{a_c} \int_0^{b_c} [B_{rs}]^T [D_{s5}][B_{rs}]\ dxdy,$$

$$\left[K^e_{rb\varphi4\_p}\right] = \int_0^a \int_0^b [B_{rb}]^T [D_{b\varphi4}][B_{\varphi}]\ dxdy,$$

$$\left[K^e_{rb\varphi4\_h}\right] = \int_0^{a_c} \int_0^{b_c} [B_{rb}]^T [D_{b\varphi4}][B_{\varphi}]\ dxdy,$$

$$\left[K^e_{r\varphi s3\_p}\right] = \int_0^a \int_0^b [B_{rs}]^T [D_{s\varphi3}][B_{\varphi}]\ dxdy,$$

$$\left[K^e_{r\varphi s3\_h}\right] = \int_0^{a_c} \int_0^{b_c} [B_{rs}]^T [D_{s\varphi3}][B_{\varphi}]\ dxdy,$$

$$\left[K^e_{rb\psi4\_p}\right] = \int_0^a \int_0^b [B_{rb}]^T [D_{b\psi4}][B_{\psi}]\ dxdy,$$

$$\left[K^e_{rb\psi4\_h}\right] = \int_0^{a_c} \int_0^{b_c} [B_{rb}]^T [D_{b\psi4}][B_{\psi}]\ dxdy,$$

$$\left[K^e_{r\psi s3\_p}\right] = \int_0^a \int_0^b [B_{rs}]^T [D_{s\psi3}][B_{\psi}]\ dxdy,$$

$$\left[K^e_{r\psi s3\_h}\right] = \int_0^{a_c} \int_0^{b_c} [B_{rs}]^T [D_{s\psi3}][B_{\psi}]\ dxdy,$$

$$\left[K^e_{rrb5\_p}\right] = \int_0^a \int_0^b [B_{rb}]^T [D_{b5}][B_{rb}]\ dxdy,$$

$$\left[K^e_{rrb5\_h}\right] = \int_0^{a_c} \int_0^{b_c} [B_{rb}]^T [D_{b5}][B_{rb}]\ dxdy,$$

$$\left[K^e_{rrb7\_p}\right] = \int_0^a \int_0^b [B_{rb}]^T [D_{b7}][B_{rb}]\ dxdy,$$

$$\left[K^e_{rrb7\_h}\right] = \int_0^{a_c} \int_0^{b_c} [B_{rb}]^T [D_{b7}][B_{rb}]\ dxdy$$

$$\left[K^e_{rrb3\_p}\right] = \int_0^a \int_0^b [B_{rb}]^T [D_{b3}][B_{rb}]\ dxdy,$$

$$\left[K^e_{rrb3\_h}\right] = \int_0^{a_c} \int_0^{b_c} [B_{rb}]^T [D_{b3}][B_{rb}]\ dxdy,$$

$$\left[K^e_{rrs1\_p}\right] = \int_0^a \int_0^b [B_{rs}]^T [D_{s1}][B_{rs}]\ dxdy,$$

$$\left[K^e_{rrs1\_h}\right] = \int_0^{a_c} \int_0^{b_c} [B_{rs}]^T [D_{s1}][B_{rs}]\ dxdy,$$

$$\left[K^e_{rrs3\_p}\right] = \int_0^a \int_0^b [B_{rs}]^T [D_{s3}][B_{rs}]\ dxdy,$$

$$\left[K^e_{rrs3\_h}\right] = \int_0^{a_c} \int_0^{b_c} [B_{rs}]^T [D_{s3}][B_{rs}]\ dxdy,$$

$$\left[K^e_{rrs5\_p}\right] = \int_0^a \int_0^b [B_{rs}]^T [D_{s5}][B_{rs}]\ dxdy,$$

$$\left[K^e_{rrs5\_h}\right] = \int_0^{a_c} \int_0^{b_c} [B_{rs}]^T [D_{s5}][B_{rs}]\ dxdy,$$

$$\left[K^e_{rb\varphi2\_p}\right] = \int_0^a \int_0^b [B_{rb}]^T [D_{b\varphi2}][B_{\varphi}]\ dxdy,$$

$$\left[K^e_{rb\varphi2\_h}\right] = \int_0^{a_c} \int_0^{b_c} [B_{rb}]^T [D_{b\varphi2}][B_{\varphi}]\ dxdy,$$

$$\left[K^e_{rb\varphi4\_p}\right] = \int_0^a \int_0^b [B_{rb}]^T [D_{b\varphi4}][B_{\varphi}]\ dxdy,$$

$$\left[K^e_{rb\varphi4\_h}\right] = \int_0^{a_c} \int_0^{b_c} [B_{rb}]^T [D_{b\varphi4}][B_{\varphi}]\ dxdy$$

$$\left[K^e_{rb\psi2\_p}\right] = \int_0^a \int_0^b [B_{rb}]^T [D_{b\psi2}][B_{\psi}]\ dxdy,$$

$$\left[K^e_{rb\psi2\_h}\right] = \int_0^{a_c} \int_0^{b_c} [B_{rb}]^T [D_{b\psi2}][B_{\psi}]\ dxdy,$$

$$\left[K^e_{rb\psi4\_p}\right] = \int_0^a \int_0^b [B_{rb}]^T [D_{b\psi4}][B_{\psi}]\ dxdy,$$

$$\left[K^e_{rb\psi4\_h}\right] = \int_0^{a_c} \int_0^{b_c} [B_{rb}]^T [D_{b\psi4}][B_{\psi}]\ dxdy,$$

$$\left[K^e_{r\varphi s1\_p}\right] = \int_0^a \int_0^b [B_{rs}]^T [D_{s\varphi1}][B_{\varphi}]\ dxdy,$$

$$\left[K^e_{r\varphi s1\_h}\right] = \int_0^{a_c} \int_0^{b_c} [B_{rs}]^T [D_{s\varphi1}][B_{\varphi}]\ dxdy,$$

$$\left[K^e_{r\varphi s3\_p}\right] = \int_0^a \int_0^b [B_{rs}]^T [D_{s\varphi3}][B_{\varphi}]\ dxdy,$$

$$\left[K^e_{r\varphi s3\_h}\right] = \int_0^{a_c} \int_0^{b_c} [B_{rs}]^T [D_{s\varphi3}][B_{\varphi}]\ dxdy,$$

$$\left[K^e_{r\psi s1\_p}\right] = \int_0^a \int_0^b [B_{rs}]^T [D_{s\psi1}][B_{\psi}]\ dxdy,$$

$$\left[K^e_{r\psi s1\_h}\right] = \int_0^{a_c} \int_0^{b_c} [B_{rs}]^T [D_{s\psi1}][B_{\psi}]\ dxdy,$$

$$\left[K^e_{r\psi s3\_p}\right] = \int_0^a \int_0^b [B_{rs}]^T [D_{s\psi3}][B_{\psi}]\ dxdy,$$

$$\left[K^e_{r\psi s3\_h}\right] = \int_0^{a_c} \int_0^{b_c} [B_{rs}]^T [D_{s\psi3}][B_{\psi}]\ dxdy,$$

$$\left[K^e_{rts1\_p}\right] = \int_0^a \int_0^b [B_{rs}]^T [D_{s1}][B_{ts}]\ dxdy,$$

$$\left[K^e_{rts1\_h}\right] = \int_0^{a_c} \int_0^{b_c} [B_{rs}]^T [D_{s1}][B_{ts}]\ dxdy,$$

$$\left[K^e_{rts3\_p}\right] = \int_0^a \int_0^b [B_{rs}]^T [D_{s3}][B_{ts}]\ dxdy,$$

$$\left[K^e_{rts3\_h}\right] = \int_0^{a_c} \int_0^{b_c} [B_{rs}]^T [D_{s3}][B_{ts}]\ dxdy,$$

$$\left[K^e_{rtb2\_p}\right] = \int_0^a \int_0^b [B_{rb}]^T [D_{b2}][B_{tb}]\ dxdy,$$

$$\left[K^e_{rtb2\_h}\right] = \int_0^{a_c} \int_0^{b_c} [B_{rb}]^T [D_{b2}][B_{tb}]\ dxdy$$

(A-7)

where, the sub-scripts p and h denote that the stiffness matrix related to MEE plate without cut-out and stiffness matrix of cut-out region only, respectively.

The various rigidity matrices contributing to Eq. (A-7) can be denoted as follows:

$$[D_{b1}] = \sum_{n=1}^{N} \int_{h_n}^{h_{n+1}} [C_b]^n \, dz, \; [D_{b2}] = \sum_{n=1}^{N} \int_{h_n}^{h_{n+1}} z[C_b]^n \, dz,$$

$$[D_{b3}] = \sum_{n=1}^{N} \int_{h_n}^{h_{n+1}} z^2[C_b]^n \, dz$$

$$[D_{b4}] = \sum_{n=1}^{N} \int_{h_n}^{h_{n+1}} c_1 z^3[C_b]^n \, dz,$$

$$[D_{b5}] = \sum_{n=1}^{N} \int_{h_n}^{h_{n+1}} c_1 z^4[C_b]^n \, dz, \; [D_{b5}] = \sum_{n=1}^{N} \int_{h_n}^{h_{n+1}} c_1 z^4[C_b]^n \, dz$$

$$[D_{b\varphi 1}] = \sum_{n=1}^{N} \int_{h_n}^{h_{n+1}} [e_b]^n \, dz, \; [D_{b\varphi 2}] = \sum_{n=1}^{N} \int_{h_n}^{h_{n+1}} z[e_b]^n \, dz,$$

$$[D_{b\varphi 4}] = \sum_{n=1}^{N} \int_{h_n}^{h_{n+1}} c_1 z^3[e_b]^n \, dz$$

$$[D_{b\psi 1}] = \sum_{n=1}^{N} \int_{h_n}^{h_{n+1}} [q_b]^n \, dz, \; [D_{b\psi 2}] = \sum_{n=1}^{N} \int_{h_n}^{h_{n+1}} z[q_b]^n \, dz,$$

$$[D_{b\psi 4}] = \sum_{n=1}^{N} \int_{h_n}^{h_{n+1}} c_1 z^3[q_b]^n \, dz, \; [D_{s1}] = \sum_{n=1}^{N} \int_{h_n}^{h_{n+1}} [C_s]^n \, dz,$$

$$[D_{s3}] = \sum_{n=1}^{N} \int_{h_n}^{h_{n+1}} c_2 z^2[C_s]^n dz \; , \; [D_{s5}] = \sum_{n=1}^{N} \int_{h_n}^{h_{n+1}} {c_2}^2 z^4[C_s]^n dz,$$

$$[D_{s\varphi 1}] = \sum_{n=1}^{N} \int_{h_n}^{h_{n+1}} [e_s]^n \, dz$$

$$[D_{s\varphi 3}] = \sum_{n=1}^{N} \int_{h_n}^{h_{n+1}} c_2 z^2[e_s]^n \, dz, \; [D_{s\psi 1}] = \sum_{n=1}^{N} \int_{h_n}^{h_{n+1}} [q_s]^n \, dz,$$

$$[D_{s\psi 3}] = \sum_{n=1}^{N} \int_{h_n}^{h_{n+1}} c_2 z^2[q_s]^n \, dz, \; [D_{\varphi\varphi}] = \sum_{n=1}^{N} \int_{h_n}^{h_{n+1}} [\eta]^n \, dz;$$

$$[D_{\psi\psi}] = \sum_{n=1}^{N} \int_{h_n}^{h_{n+1}} [\mu]^n \, dz,$$

$$[D_{\varphi\psi}] = \sum_{n=1}^{N} \int_{h_n}^{h_{n+1}} [m]^n \, dz \tag{A-8}$$

The condensation procedure adopted to obtain Eq. (A-5) from Eqs. (A-1)–(A-4) can be found in authors' own work [35].

References

[1] Vinyas M, Kattimani SC. Investigation of the effect of $BaTiO_3/CoFe_2O_4$ particle arrangement on the static response of magneto-electro-thermo-elastic plates. Compos Struct 2018a;185:51–64.

[2] Vinyas M, Kattimani SC, Loja MAR, Vishwas M. Effect of BaTiO3/CoFe2O4 micro-topological textures on the coupled static behaviour of magneto-electro-thermo-elastic beams in different thermal environment. Mater Res Express 2018a;5:125702.

[3] Vinyas M, Kattimani SC, Sharanappa J. Hygrothermal coupling analysis of magneto-electro-elastic beams using finite element methods. J Therm Stresses 2018;4 1(8):1063–79.

[4] Vinyas M, Kattimani SC. Static studies of stepped functionally graded magneto-electro-elastic beam subjected to different thermal loads. Compos Struct 2017;163:216–37.

[5] Vinyas M, Kattimani SC. A Finite element based assessment of static behavior of multiphase magneto-electro-elastic beams under different thermal loading". Struct Eng Mech 2017;62:519–35.

[6] Vinyas M, Kattimani SC. Static behavior of thermally loaded multilayered magneto-electro-elastic beam. Struct Eng Mech 2017;63(4):481–95.

[7] Vinyas M, Kattimani SC. Static analysis of stepped functionally graded magneto-electro-elastic plates in thermal environment: a finite element study. Compos Struct 2017;178:63–86.

[8] Vinyas M, Kattimani SC. Hygrothermal analysis of magneto-electro-elastic plate using 3D finite element analysis. Compos Struct 2017;180:617–37.

[9] Pan E. Exact solution for simply supported and multilayered magneto-electro-elastic plates. J Appl Mech 2001;68:608–18.

[10] Pan E, Heyliger PR. Free vibrations of simply supported and multilayered magneto-electro-elastic plates. J Sound Vib 2002;252(3):429–42.

[11] Wang J, Chen L, Fang S. State vector approach to analysis of multilayered magneto-electro-elastic plates. Int J Solid Struct 2003;40(7):1669–80.

[12] Chen JY, Heyliger PR, Pan E. Free vibration of three-dimensional multilayered magneto-electro-elastic plates under combined clamped/free boundary conditions. J Sound Vib 2014;333(17):4017–29.

[13] Lage RG, Soares CM, Soares CA, Reddy JN. Layerwise partial mixed finite element analysis of magneto-electro-elastic plates. Comput Struct 2004;82(17):1293–301.

[14] Ramirez F, Heyliger PR, Pan E. Free vibration response of two-dimensional magneto-electro-elastic laminated plates. J Sound Vib 2006;292(3):626–44.

[15] Huang DJ, Ding HJ, Chen WQ. Analytical solution for functionally graded magneto-electro-elastic plane beams. Int J Eng Sci 2007;45(2):467–85.

[16] Bhangale RK, Ganesan N. Free vibration of simply supported functionally graded and layered magneto-electro-elastic plates by finite element method. J Sound Vib 2006;294(4):1016–38.

[17] Annigeri AR, Ganesan N, Swarnamani S. Free vibration behavior of multiphase and layered magneto-electro-elastic beam. J Sound Vib 2007;299(1):44–63.

[18] Daga A, Ganesan N, Shankar K. Behavior of magneto-electro-elastic sensors under transient mechanical loading. Sens Actuators, A 2009;150(1):46–55.

[19] Sladek J, Sladek V, Krahulec S, Pan E. The MLPG analyses of large deflections of magnetoelectroelastic plates. Eng Anal Bound Elem 2013a;37(4):673–82.

[20] Chen WQ, Lee KY. Alternative state space formulations for magnetoelectric thermoelasticity with transverse isotropy and the application to bending analysis of nonhomogeneous plates. Int J Solid Struct 2003;40(21):5689–705.

[21] Chen WQ, Lee KY, Ding HJ. On free vibration of non-homogeneous transversely isotropic magneto-electro-elastic plates. J Sound Vib 2005;279(1–2):237–51.

[22] Xin L, Hu Z. Free vibration of simply supported and multilayered magneto-electro-elastic plates. Compos Struct 2015;121:344–50.

[23] Vinyas M, Harursampath D, Trung NT. Influence of active constrained layer damping on the coupled vibration response of functionally graded magneto-electro-elastic plates with skewed edges. Defence Technology; 2019. https://doi.org/10.1016/j.dt.2019.11.016.

[24] Vinyas M, Kattimani SC. Finite element simulation of controlled frequency response of skewed multiphase magneto-electro-elastic plates". J Intell Mater Syst Struct 2019;30(12):1757–71.

[25] Vinyas M. Vibration control of skew magneto-electro-elastic plates using active constrained layer damping. Compos Struct 2019;208:600–17.

[26] Vinyas M. Interphase effect on the controlled frequency response of three-phase smart magneto-electro-elastic plates embedded with active constrained layer damping: FE study. Materials Research Express; 2019. https://doi.org/10.1088/2053-1591/ab6649.

[27] Vinyas M, Piyush JS, Kattimani SC. Influence of coupled fields on free vibration and static behavior of functionally graded magneto-electro-thermo-elastic plate. J Intell Mater Syst Struct 2018a;29(7):1430–55.

[28] Moita JMS, Soares CMM, Soares CAM. Analyses of magneto-electro-elastic plates using a higher order finite element model. Compos Struct 2009;91(4):421–6.

[29] Shooshtari A, Razavi S. Vibration analysis of a magnetoelectroelastic rectangular plate based on a higher-order shear deformation theory. Lat Am J Solid Struct 2016;13(3):554–72.

[30] Vinyas M, Kattimani SC. Finite element evaluation of free vibration characteristics of magneto-electro-elastic plates in hygrothermal environment using higher order shear deformation theory. Compos Struct 2018b;202:1339–52.

[31] Vinyas M, Kattimani SC, Harursampath D, Nguyen Thoi-T. Coupled evaluation of the free vibration characteristics of magneto-electro-elastic skew plates in hygrothermal environment. Smart Struct Syst 2019;24(2):267–92.

[32] Vinyas M, Nischith G, Loja MAR, Ebrahimi F, Duc ND. Numerical analysis of the vibration response of skew magneto-electro-elastic plates based on the higher-order shear deformation theory. Compos Struct 2019;214:132–42.

[33] Vinyas, M.A higher order free vibration analysis of carbon nanotube-reinforced magneto-electro-elastic plates using finite element methods.

Composites Part B, 158, 286-301.
[34] Vinyas M, Sunny KK, Harursampath D, Trung NT, Loja MAR. Influence of interphase on the multi-physics coupled frequency of three phase smart magneto-electro-elastic composite plates. Compos Struct 2019;226:111254.
[35] Vinyas M, Sandeep AS, Trung NT, Ebrahimi F, Duc ND. A finite element based assessment of free vibration behaviour of circular and annular magneto-electro-elastic plates using higher order shear deformation theory. J Intell Mater Syst Struct 2019;30(6):2478–501.
[36] [a] Grossi RO, Laura PAA, Arenas B del V. Free vibration of rectangular plates with circular openings. Ocean Eng 1997;24(1):19–24.[b] Lam KY, Hung KC, Chow ST. Vibration analysis of plates with cutouts by the modified Rayleigh-Ritz method. Appl Acoust 1989;28:49–60.
[37] Lee HP, Lim SP, Chow ST. Prediction of natural frequencies of rectangular plates with rectangular cutouts. Comput Times 1990;36(5):861–9.
[38] Masia U, Avalos DR, Laura PAA. Displacement amplitudes and flexural moments for a rectangular plate with a rectangular cutout under a uniformly distributed static load. J Sound Vib 2005;280:433–42.
[39] Boay CG. Free vibration of laminated composite plates with a central circular hole. Compos Struct 1996;35(4):357–68.
[40] Ramakrishna S, Rao KM, Rao NS. Free vibration analysis of laminates with circular cutout by hybrid-stress finite element. Compos Struct 1992;21:177–85.
[41] Huang M, T S. Free vibration analysis of rectangular plates with variously -shaped holes. J Sound Vib 1999;226(4):769–86.
[42] Lee HP, Lim SP. Free vibration of isotropic and orthotropic square plates with square cutouts subjected to in-plane forces. Comput Struct 1992;43(3):431–7.
[43] Huang DT. Effects of constraint , circular cutout and in-plane loading on vibration of rectangular plates. Int J Mech Sci 2013;68:114–24.
[44] Lee HP, Lim SP, Chow ST. Effect of transverse shear deformation and rotary inertia on the natural frequencies of rectangular plates with cutouts. Int J Solid Struct 1992;29(11):1351–9.
[45] Nguyen V, Do V, Lee C. Free vibration analysis of FGM plates with complex cutouts by using quasi-3D isogeometric approach. Int J Mech Sci 2019;159:213–33.
[46] Wang G, Li W, Feng Z, Ni J. A unified approach for predicting the free vibration of an elastically restrained plate with arbitrary holes. Int J Mech Sci 2019;159:267–77.
[47] Andrianov IV, Danishevs'Kyy VV, Kalamkarov AL. Asymptotic analysis of perforated plates and membranes. Part 2: static and dynamic problems for large holes. Int J Solid Struct 2012;49(2):311–7.
[48] Chen YC, Hwu C. Boundary element method for vibration analysis of two-dimensional anisotropic elastic solids containing holes, cracks or interfaces. Eng Anal Bound Elem 2014;40:22–35.
[49] Chen Y, Jin G, Liu Z. Flexural and in-plane vibration analysis of elastically restrained thin rectangular plate with cutout using Chebyshev-Lagrangian method. Int J Mech Sci 2014;89:264–78.
[50] Hota SS, Padhi P. Vibration of plates with arbitrary shapes of cutouts. J Sound Vib 2007;302:1030–6.
[51] Kwak MK, Han S. Free vibration analysis of rectangular plate with a hole by means of independent coordinate coupling method. J Sound Vib 2007;306:12–30.
[52] Liew KM, Kitipornchai S, Leung AYT, Lim CW. Analysis of the free vibration of rectangular plates with central cut-outs using the discrete Ritz method. Int J Mech Sci 2003;45:941–59.
[53] Mondal S, Patra AK, Chakraborty S, Mitra N. Dynamic performance of sandwich composite plates with circular hole/cut-out: a mixed experimental – numerical study. Compos Struct 2015;131:479–89.
[54] Shufrin I, Eisenberger M. Semi-analytical modeling of cutouts in rectangular plates with variable thickness – free vibration analysis. Appl Math Model 2016:1–18. 0.
[55] Huang B, Wang J, Du J, Ma T, Guo Y, Qian Z. Vibration analysis of a specially orthotropic composite laminate with rectangular cutout using independent coordinate coupling method. Compos Struct 2016;150:53–61.
[56] Lee S. Finite element dynamic stability analysis of laminated composite skew plates containing cutouts based on HSDT. Compos Sci Technol 2010;70(8):1249–57.
[57] Park T, Lee S, Voyiadjis GZ. Finite element vibration analysis of composite skew laminates containing delaminations around quadrilateral cutouts. Compos Part B 2009;40(3):225–36.
[58] Natarajan S, Deogekar PS, Manickam G, Belouettar S. Hygrothermal effects on the free vibration and buckling of laminated composites with cutouts. Compos Struct 2014;108:848–55.
[59] Venkatachari A, Natarajan S, Haboussi M. Environmental effects on the free vibration of curvilinear fibre composite laminates with cutouts. Compos Part B 2016;88:131–8.
[60] Ovesy HR, Fazilati J. Buckling and free vibration finite strip analysis of composite plates with cutout based on two different modeling approaches. Compos Struct 2012;94(3):1250–8.
[61] Zhang YP, Wang CM, Pedroso DM, Zhang H. Extension of Hencky bar-net model for vibration analysis of rectangular plates with rectangular cutouts. J Sound Vib 2018;432:65–87.
[62] Areias P, Rabczuk T, Msekh M. Phase-field analysis of finite-strain plates and shells including element subdivision. Comput Methods Appl Mech Eng 2016;312:322–50.
[63] Areias P, Rabczuk T, de Sá JC, Soares CM. Fully-coupled piezoelectric assumed-strain least-squares nonlinear shell. Thin-Walled Struct 2018;131:631–45.
[64] Chikkol Venkateshappa S, Kumar P, Ekbote T. CEAS Aeronaut J 2019;10:623. https://doi.org/10.1007/s13272-018-0339-7.